In-situ laboratory X-ray diffraction applied to assess cement hydration

Paulo R. de Matos [1,*]; José S. Andrade Neto [2]; Daniel Jansen [3]; Angeles G. De la Torre [4]; Ana Paula Kirchheim [2]; Carlos E. M. Campos [5].

[1] Coordenadoria Acadêmica, Campus Cachoeira do Sul, Federal University of Santa Maria (UFSM), Brazil.

[2] Núcleo Orientado para Inovação da Edificação (NORIE), Universidade Federal do Rio Grande do Sul (UFRGS), Brazil.

[3] Friedrich-Alexander University Erlangen-Nuernberg, GeoZentrum Nordbayern, Mineralogy, Schlossgarten 5a, 91054 Erlangen, Germany.

[4] Departamento de Química Inorgánica, Cristalografía y Mineralogía, Universidad de Malaga (UMA), Campus Teatinos s/n., 29071 Málaga, Spain.

[5] Departamento de Física, Federal University of Santa Catarina (UFSC), Brazil.

* corresponding author (paulo.matos@ufsm.br).

Abstract

In-situ X-ray diffraction (XRD) is a powerful tool to assess the hydration of cementitious materials, providing time-resolved quantitative analysis with reasonable accuracy without disturbing sample. However, the lack of guidelines and well-established procedures for data collection and analysis is the limiting factor for spreading this technique. This paper discussed using *in-situ* laboratory XRD to assess cement hydration. The first part was dedicated to a literature review on the topic. Then, experimental strategies were discussed, and recommendations related to the data analysis routine were drawn; the advantages and limitations of this technique were also discussed. We can conclude that the critical factors for a successful analysis are the choice of an adequate experimental setup with good statistics and low measurement time, the proper consideration of different amorphous contributions in the XRD pattern, and a good data analysis routine. Independent techniques are highly recommended to support the *in-situ* XRD data.

Keywords: X-ray diffraction; *in-situ* XRD; laboratory XRD; cement; hydration.

1. Introduction

Portland cement is the most consumed manufactured material globally, with an average production of 4.6 Gt per year. Although its invention dates back approximately 200 years (patent GB 5022 granted in 1824), we still do not fully understand its reaction mechanisms – the so-called hydration reactions [1]. Therefore, in addition to Portland cement (PC), alternative cements have emerged to reduce the environmental impact caused by PC production, which releases 0.8-1.0 tons of CO_2 for each ton of clinker produced and is responsible for about 8% of the global CO_2 emission [2]. Among these alternative cements, calcium (sulfo)aluminate [3,4], belitic [5,6], sulfobelitic or belite-ye'elimite-ferrite (BYF) [7,8], magnesia-based [5], and alkali-activated cements [4,8] stand out. Another popular approach for reducing the CO_2 emission associated with cement production is replacing high levels of Portland clinker with supplementary cementitious materials (SCMs). For instance, limestone calcined clay cements (LC^3) allow about 50% clinker replacement with equivalent performance to PC [9].

These cements progressively react with water (or alkaline solution) to form new phase assemblage, filling space and developing mechanical properties. This process is based on the simultaneous dissolution of anhydrous cement compounds and precipitation of solid phases. The kinetics of these reactions as well as the type and content of the products formed, affect both the fresh (*e.g.*, rheology and setting time) and the hardened properties of the material (*e.g.*, porosity, mechanical strength, and durability). Therefore, it is crucial to study the phase assemblage of cementitious systems over time. However, each cement is composed of different phases and forms various products with different kinetics, making it difficult to properly quantify and characterize the phases present in these cementitious systems over time.

The evolution of equipment and analytical techniques has allowed new insights into the reaction mechanisms of different cements. X-ray diffraction (XRD) is one of the most used techniques in order to evaluate the phase composition of anhydrous and hydrated cementitious materials. It (usually) allows quantitative phase analysis (QPA) with reasonable accuracy while small amounts of sample and low testing times (as low as 10 minutes) are required [10]. Besides, XRD provides QPA results that agree well with independent methods such as thermogravimetric analysis (TGA) [10,11], isothermal calorimetry [12], scanning electron microscopy (SEM) [10], and nuclear magnetic resonance (NMR) [13,14]. The progress achieved in terms of equipment and software made XRD popular, from laboratory research to cement plants for quality control of clinker production [13]. Currently, there is a variety in equipment size, analysis capability and price, from benchtop diffractometers less than a meter in size costing tens of thousands of dollars to synchrotron facilities with hundreds of meters in size, costing hundreds of millions of dollars.

Time-resolved measurements are of great interest in cement research since they provide continuous information on reacting systems with little sample disturbance and no additional sample preparation, *i.e.*, hydration stoppage and grinding. Techniques such as isothermal calorimetry provide continuous measurements with good reproducibility, but it only gives an overall look at the hydration

kinetics. Since different reactions occur simultaneously during cement hydration, methods like isothermal calorimetry do not allow separating between different dissolution and precipitation reactions which run synchronously during hydration. In contrast, *in-situ* XRD can provide the individual content of each phase in the system over time and consequently, each dissolution and precipitation reaction can be followed, provided that the phases dissolved or formed are crystalline. Synchrotron XRD has been successfully used in recent years for *in-situ* analysis of hydrating cements [15–21]. Although synchrotron XRD provides high-quality data with a short measurement time, the equipment involved are very expensive, which limits access to them. In fact, there are currently less than 100 synchrotron facilities worldwide. In turn, laboratory X-ray diffractometers are far more affordable and can also provide *in-situ* quantitative measurements.

Figure 1 shows the number of articles published in the past year addressing *in-situ* laboratory XRD applied to cement-based materials; full data is available in Supplementary File. The use of this technique for cement-based materials is relatively new and is growing fast; however, it is still restricted to a few research groups due to the complexity of data analysis. This occurs even though the experimental setup required for *in-situ* experiments is not that different from powder XRD (discussed in Section 2.2), so the lack of guidelines and well-established procedures for data collection and analysis is the limiting factor for further spreading the use of this technique.

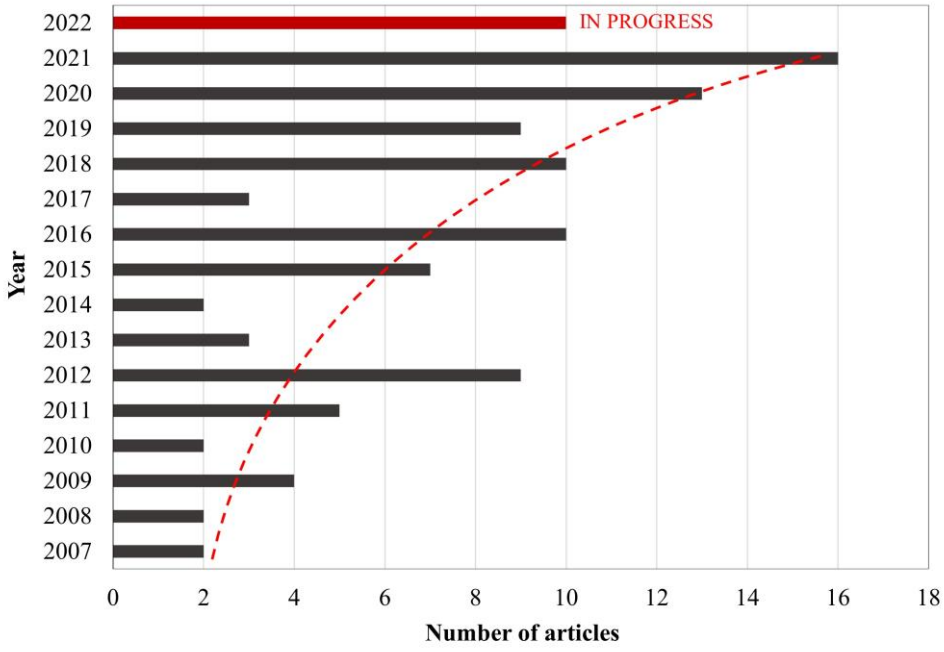

Figure 1. Articles published in the past years addressing *in-situ* laboratory XRD applied for cement-based materials. Result for Scopus database search in August 2022 for ("in situ XRD" OR "in-situ XRD") AND ("cement" or "C3S" or "alite" or "C3A" or "ye'elimite" or "alkali-activated") in the title, keywords, or abstract. Note: it only considers laboratory XRD studies related to cement hydration.

In this context, the current paper discusses the use of *in-situ* laboratory XRD (hereafter called *in-situ* XRD) applied to assess cement hydration. Section 2 presents a literature review on the current

applications (Section 2.1) and summarizes the testing conditions reported (Section 2.2). Sections 3-5 discuss the appropriate experimental procedures and data analysis strategies, besides drawing recommendations for the refinement routine. The limitations and advantages of using this technique alone and in combination with other analytical methods are also discussed.

2. Current applications and experimental settings

Several studies have used *in-situ* XRD to follow the reaction of different cements over time. Section **Erro! Fonte de referência não encontrada.** presents a literature review of the main findings on the use of *in-situ* XRD applied to cement-based materials. The experimental conditions used in these previous studies are summarized and discussed in Section 2.2.

2.1. Literature review

2.1.1. Pure cement phases

Valentini *et al.* [22] studied the hydration of pure C_3S in the absence and the presence of gypsum over the first 12.5 hours of hydration. The authors observed that the addition of gypsum accelerated the hydration degree of C_3S and the C-S-H formation after the onset of the acceleration period, confirming what Mota et al. [23] observed earlier without XRD. By combining the amorphous content obtained by the G-factor method (see Section 3.3) and mass balance calculations, the authors suggested that a significant amount of SO_4^{2-} are incorporated in C-S-H by surface adsorption. Similarly, Bergold *et al.* [24] followed the first 35 hours of the hydration of a synthesized monoclinic C_3S through *in-situ* XRD and isothermal calorimetry, observing that the crystallite size of C-S-H remained unchanged (ranging within 7.7-9.1 nm) from the first formation of C-S-H until the end of the experiments. They also observed that C-S-H formation did not occur fully synchronized with C_3S dissolution, indicating the formation of an intermediate phase, *i.e.*, a short-range ordered C-S-H non-detectable by XRD before forming long-range ordered C-S-H nanostructure. These findings corroborate Jennings' C-S-H model [25–27], where its growth occurs by the aggregation of "particles", which was recently confirmed by Plank *et al.* [28] using transmission electron microscopy.

Quennoz and Scrivener [29] conducted one of the first *in-situ* investigations on the hydration of C_3A-gypsum systems. *In-situ* XRD confirmed that the solid gypsum depletion leads to renewed and fast C_3A dissolution and ettringite consumption for monosulfate formation. Kirchheim *et al.* [30] evaluated the first 15 hours of hydration of cubic and orthorhombic C_3A pastes with different amounts of gypsum by *in-situ* XRD and isothermal calorimetry. It was observed that the orthorhombic C_3A reacted much faster in the presence of gypsum, presenting faster ettringite formation, as well as faster gypsum and C_3A consumption compared with cubic C_3A pastes. Andrade Neto *et al.* [31] evaluated the hydration of cubic, cubic + NaOH, and Na-doped orthorhombic C_3A in the presence of gypsum and hemihydrate using *in-situ* XRD together with isothermal calorimetry and TGA. The authors observed that orthorhombic C_3A had a faster dissolution, with quicker ettringite formation and sulfate depletion. In turn, the addition of NaOH in the solution did not influence the hydration of cubic C_3A

in the first 20 hours. Thus, the XRD results coupled with calorimetry indicated that the higher reactivity of orthorhombic C_3A is due to the change in the crystalline structure rather than the presence of sodium in the solution. This trend was also observed by Wistuba *et al.* [32] when evaluating four white Portland cements with different amounts of Na_2O in the clinker through *in-situ* XRD. Additionally, the authors found that the Na doping delayed the formation of crystalline ettringite and monosulfate during the first few hours of hydration.

Cai *et al.* [33] analyzed the effect of seawater as mixing water on the hydration of cubic C_3A through *in-situ* and powder XRD, in addition to complementary techniques. It was observed that the seawater retarded C_3A hydration mainly due to the ion-pairing of Ca^{2+} and SO_4^{2-} onto the surface of C_3A, as previously suggested by Myers et al. [34] by using different techniques such as zeta potential measurements and X-ray absorption spectroscopy (XAS). Besides, the precipitation of $Mg(OH)_2$ on the surface of C_3A also contributed to the delay in the C_3A reaction. Finally, the presence of Cl^- ions in the seawater led to Friedel´s salt formation instead of hydroxy-AFm (the latter, observed in the paste produced with deionized water). Ectors *et al.* [35] studied the hydration of synthetic brownmillerite (C_4AF) in the presence of low Ca-sulfate content and calcite by quantitative *in-situ* XRD and calorimetry. The authors observed a similar behavior to the C_3A pastes mentioned before [29–31]: a first initial reaction due to the rapid dissolution of bassanite and C_4AF forming ettringite, followed by a period with low heat release where the dissolution of anhydrite and the formation of ettringite slowly continue. Then, a few hours after the complete anhydrite dissolution and ettringite maximum formation, C_4AF started to dissolve again, while ettringite became unstable, and the AFm phases started to form.

In-situ XRD can also be used to assess the effect of doping cement phases on their hydration. Souza *et al.* [36] doped C_3S with ZnO, evaluating the phase formation and hydration, respectively, through powder and *in-situ* XRD. The authors observed that adding up to 2 wt% ZnO in the raw mix for cements synthesized at 1300°C, and up to 4 wt% ZnO for cements synthesized at 1500°C did not retard the cement hydration. Andrade Neto *et al.* [37] assessed the effect of doping C_3S and C_3A, respectively, with Al_2O_3 and Na_2O, on the hydration of C_3S-C_3A-calcium sulfate systems using *in-situ* XRD. The authors found that the aluminum presence in C_3S was the most impactful factor, leading to further and faster ettringite formation, anticipating gypsum depletion, and increasing the sulfate demand of the mixes. Na_2O doping on C_3A also increased the sulfate demand of the systems but to a lesser extent.

Besides Andrade Neto *et al.* [37], other studies used *in-situ* XRD to evaluate C_3S-C_3A-calcium sulfate systems. Hesse *et al.* [38,39] conducted one of the first *in-situ* studies on these systems, evaluating the hydration of 95% C_3S + 5% cubic C_3A samples in the presence of anhydrite and bassanite. Isothermal calorimetry and *in-situ* XRD were conducted. The authors calculated the hydration heat released by the samples through the enthalpies of the dissolution of the anhydrous phases and the formation of the hydrate phases. The key findings were: (*i*) the great heat release in the first minutes is due to the aluminate reaction; (*ii*) the main heat release period is dominated by the

silicate reaction; and (*iii*) the second and less intense heat flow peak (known as shoulder peak), is attributed to a new fast C_3A dissolution with the final formation of ettringite. Finally, the authors observed that the dissolution of C_3A is controlled by the availability of the calcium sulfate phases. Similarly, Quennoz and Scrivener [40] studied C_3S and C_3A-gypsum hydration interactions by *in-situ* XRD, calorimetry, and SEM. *In-situ* XRD results confirmed that C_3A slowly dissolves during the first hours, while gypsum is dissolved and ettringite is formed quicker. When all solid gypsum is consumed, the C_3A dissolution rate increases abruptly, and the ettringite formation rate increases. Zunino and Scrivener [41] evaluated the hydration of C_3S-C_3A-calcium sulfate systems, varying the fineness of the materials, through *in-situ* XRD, calorimetry, and SEM. XRD revealed that the amount of ettringite precipitated before the sulfate depletion and the adsorption of sulfate into C-S-H are the main factors influencing the sulfate balance of the studied systems: the C_3S fineness influenced the C-S-H precipitation ratio, while the C_3A fineness modified the amount of ettringite precipitated.

2.1.2. Ordinary and blended Portland cements

In-situ XRD has also been successfully applied to study the hydration of commercial Portland and blended cements (*i.e.*, containing SCM) [10,42,43]. Jansen and co-authors conducted several studies on this topic. In Ref. [44], they proposed a remastered external standard method to determine the phase composition of hydrating cement pastes, using the "G-factor" method (detailed in Section 3.3) for quantitative phase analysis. Combining *in-situ* XRD and isothermal calorimetry results, the authors observed that significant C_3S dissolution and the portlandite precipitation only started after the end of the induction period. Regarding sulfates, they observed that gypsum is consumed faster than anhydrite. When all calcium sulfate was consumed (known as sulfate depletion), C_3A started to dissolve again, resulting in a fast ettringite precipitation. In Ref. [45], the authors evaluated the hydration of PC pastes, comparing the heat release calculated from phase dissolution/precipitation with that measured by calorimetry. The authors observed that the C_3S and C_3A dissolutions and C-S-H, portlandite, and ettringite precipitation were the main responsible for the heat release within the first 22 hours, while anhydrite and gypsum dissolutions had a small contribution to the heat release. In Ref. [46], they coupled *in-situ* XRD with pore solution and ^{1}H NMR analyses to evaluate the early hydration of PC, finding a good correlation between the techniques. The authors also observed a good agreement between the theoretical amount of hydrogen in the solid fraction (obtained by ^{1}H NMR) and that calculated by *in-situ* XRD (considering the amount of water present in C-S-H, ettringite, and portlandite). These technique associations will be further discussed in Section 5.

The effect of different sulfate contents on white PC hydration was evaluated by Berodier *et al.* [47] through *in-situ* XRD and complementary techniques. The authors observed that the sulfate content increased the ettringite content while reducing the portlandite content. They also found that when gypsum depletion occurs (observed by *in-situ* XRD), the morphology of C-S-H changes from divergent needles to agglomerated morphology (observed by SEM). This change in the C-S-H morphology evidenced that the sulfate is adsorbed onto the C-S-H in the first hours of hydration but is released when the sulfate depletion occurs, which leads to a new fast ettringite formation (confirmed

by *in-situ* XRD), proving the previous findings from Mota et al. [23]. Still regarding sulfates, Dubina *et al.* [48] observed through powder XRD that hemihydrate and arcanite reacted with the C_3A to form ettringite in "aged" PC (kept at 85% RH for 24 hours). The authors additionally used *in-situ* XRD to compare the reactivity of such aged PC with "fresh" (*i.e.*, not pre-hydrated) PC, observing that the aged cement had a lower reactivity, with a slower C_3S dissolution and portlandite formation. In turn, C_4AF was not significantly affected by the pre-hydration.

Jakob *et al.* [49] coupled *in-situ* XRD and rheological measurements to evaluate the effect of the temperature (20°C and 30°C) on the early-age behavior of PC pastes (up to 5 hours). The authors observed that the amount of ettringite greatly influenced the rheological properties of the cement paste due to the high water consumption and the change in the water/solid ratio. Furthermore, the effect of ettringite on the rheological properties of the cement paste grows exponentially with the hydration time. Finally, the ambient temperature strongly influenced the amount of ettringite formed: an increase in the temperature leads to a faster ettringite formation, increasing the yield stress of paste. Also related to temperature, Schreiner *et al.* [50] used *in-situ* XRD to assess the hydration of PC-lime-anhydrite mixes at 70ºC, which corresponds to the mean temperature usually prevailing in the industrial process during the earlier hydration (before autoclaving) of the autoclaved aerated concrete. The authors successfully applied a new approach to treat anisotropic domain sizes for portlandite and tobermorite, which was previously developed by Ectors *et al.* [51,52]. The authors observed two distinct generations of portlandite: the first due to the lime hydration, showing anisotropic peak broadening, and the second due to the C_3S hydration, which shows isotropic domain size. A biaxial cylindrical model was used for the anisotropic domain size calculation. It was shown that the "cylinder" (portlandite) height remains stable during the hydration process, but the cylinder diameter increases during the first hours of hydration.

Regarding the incorporation of SCMs, Dittrich *et al.* [53] assessed the first 44 hours of hydration of PC blended with 50 wt% of siliceous fly ash and quartz powder using *in-situ* XRD and calorimetry. Two fly ashes and quartz powders with different particle sizes were used. The use of the coarser fly ash (d_{50} = 19.2 μm) and quartz powder (d_{50} = 22.3 μm) had a minor influence on the first 44 h of hydration, while the use of the finer quartz powder (d_{50} = 2.3 μm) slightly accelerated the cement hydration. In turn, the use of the finer fly ash (d_{50} = 2.1 μm) led to a strong delay in the silicate reaction, retarding the dissolution of C_3S and the formation of C-S-H. In contrast, the use of the finer fly ash accelerated the aluminate reaction and the ettringite precipitation. De Matos *et al.* [54] evaluated the hydration of PC pastes with 0-30 wt% replacement of cement with ceramic tile demolition waste (CTDW) or limestone filler through *in-situ* XRD and calorimetry. The authors observed that the CTDW enhanced the cement hydration kinetics compared to limestone filler, leading to further C_3S consumption and ettringite and portlandite formation. These results agreed with the compressive strength results, in which the pastes with CTDW presented compressive strengths up to 5% higher than those with limestone filler. Land and Stephan [55] analyzed the influence of different nanosilica on white Portland cement hydration through *in-situ* XRD and calorimetry. The authors

observed that the addition of nanosilica led to faster consumption of C_3S and faster precipitation of portlandite. In addition, the greater the nanosilica surface area, the higher the acceleration on the C_3S hydration. Zunino and Scrivener [56] used the *in-situ* XRD and isothermal calorimetry to study the mechanism responsible for the increased sulfate demand of the LC^3. A strong linear correlation (R^2 = 0.97) between the ettringite and AFm contents obtained by *in-situ* XRD and the heat released during the aluminate peak in calorimetry was observed. They concluded that both limestone and calcined clay incorporation led to an increase in C-S-H precipitation rate due to the filler effect, and more sulfate was adsorbed by the C-S-H, accelerating the gypsum depletion. Redondo-Soto *et al.* [57] also studied PC samples containing calcined clay (67 wt% PC 42.5-R + 30 wt% metakaolin + 3 wt% gypsum), combining MoKα_1 XRD and X-ray microtomography (µ-CT). For this purpose, pastes with a w/c ratio of 0.5 were loaded in a glass capillary of 1 mm in diameter for the *in-situ* XRD study and poured into cylinders for the *ex-situ* study according to Ref. [58]. The methodology for measuring both types of data in unaltered pastes in the same region of a given capillary has been recently reported for the first time in Ref. [59]. The authors found good agreement between the techniques discussed later in Section 5.

2.1.3. Portland cement with chemical admixtures

In-situ XRD has been successfully applied to studies regarding the effect of admixtures on PC hydration. Jansen *et al.* [60] studied the effect of a polycarboxylate ether (PCE) superplasticizer on the hydration of a commercial PC using thermodynamic modeling to calculate heat flow diagrams from *in-situ* XRD data and then compared to the heat flow curves measured by isothermal calorimetry. It was shown that the superplasticizer retarded both silicate and aluminate reactions, suggesting that this retarding effect occurred due to (*i*) the complexation of Ca^{2+}; (*ii*) the adsorption of superplasticizer on the nuclei of the hydrate phases preventing their growth; and/or (*iii*) the adsorption of the macromolecules on the surfaces of the cement/clinker phases which is in line with general discussed interactions of PCEs with PCs [61,62]. Such delayed silicate reaction in the presence of PCE was also reported by Valentini *et al.* [63], which observed that PCE affected the C–S–H nucleation and growth. Furthermore, the authors observed that a delayed PCE addition (*e.g.*, after the first 4 min of mixing) prevented this phenomenon, similar to that observed by de Matos *et al.* [64] for PC and LC^3 pastes with a 10-min delay in PCE addition. Pott *et al.* [65] investigated the incompatibility between PC and PCE admixtures using *in-situ* XRD, isothermal calorimetry, rheological tests, and SEM. The authors observed that PCE accelerated the C_3A and C_4AF hydration, leading to a much faster ettringite formation and earlier hemicarbonate formation, resulting in a fast workability loss and early stiffening. This effect can be minimized by further gypsum incorporation or by delaying the PCE addition. Still regarding PCE, Kanchanason and Plank [66] evaluated the effect of self-synthesized C-S-H+PCE nanocomposite on the hydration and strength of slag and calcined clay blended cements using *in-situ* (besides other techniques), finding that C-S-H+PCE nanocomposite acts as a seeding material, accelerating both silicate and aluminate reactions and increasing the formation rate of portlandite, C-S-H, ettringite, and AFm phases.

PC hydration in the presence of polymers other than PCE was also studied using *in-situ* XRD. Jansen *et al.* [67] evaluated the effect of two different dialyzed styrene-acrylate polymer dispersion on the early hydration of PC. The polymers retarded the cement hydration, slowing the C_3S dissolution and the C-S-H precipitation, and the retarding effect was more substantial for the polymer with the lower glass transition temperature (T_g). According to the authors, the retardation of cement hydration is most likely due to the adsorption of the polymers on the cement or hydrate grains, hindering the nucleation and growth of the hydrate phases on them. Similarly, Kong *et al.* [68] investigated the effects of polymer latexes with cleaned serum on PC hydration by the combination of *in-situ* XRD, isothermal calorimetry, and Cryo-SEM. The authors observed that both polymers retard the silicate and aluminate hydration, slowing the C_3S, C_3A, gypsum, and anhydrite dissolutions, consequently delaying the formation of C-S-H and ettringite. Besides, anionic colloidal polymers had a greater retarding effect on the aluminate reaction than on the silicate, probably due to the stronger interaction between the polymer molecules and the positively charged aluminate phases. Lu *et al.* [69,70] studied the acting mechanism of triethanolamine (TEA) and diethanol-isopropanolamine (DEIPA) on PC, observing that the addition of TEA led to a retardation of C_3S dissolution, slowing the portlandite precipitation. TEA accelerated both C_3A and C_4AF reactions, resulting in faster ettringite formation and gypsum depletion. Therefore, the addition of 0.5% of TEA resulted in undersulfated systems, in which the sulfate depletion and the renewed C_3A hydration occurred before the C_3S main reaction. Comparable interaction was found with DEIPA. Additional work on TEA and PC hydration applying *in-situ* XRD was done by Hirsch et al. [71]. It was found that the impact of TEA on PC hydration is affected by the dissolution rate of sulfate carriers.

2.1.4. Calcium aluminate and sulfoaluminate cements

Some studies have used *in-situ* XRD to follow the hydration of calcium aluminate (CA) and calcium sulfoaluminate (CSA) pure phases and cements. For example, Jansen *et al.* [72] studied the hydration of synthetic ye'elimite in the presence of calcium sulfates, observing that small amounts of ye'elimite reacted within the first hours (*i.e.*, within the induction period), forming up to 5 wt% of ettringite. After the induction period (at around 2 hours of hydration), the ye'elimite dissolution rate increased, resulting in a large ettringite formation. Ma *et al.* [73] investigated the effect of adding 4 wt% ye'elimite in the C_3S clinker, using *in-situ* and powder XRD to show that ye'elimite reacted within the first 1.5 hours, leading to a great ettringite formation. As a result, the hydrated ye'elimite-doped C_3S sample had a denser matrix at one day of age than the plain C_3S sample. Wolf *et al.* [74] used *in-situ* XRD to assess the impact of incorporating Li_2CO_3 on the hydration of ternary CSA-PC-anhydrite mixes, observing that moderate contents of Li_2CO_3 (*i.e.*, up to 0.45 wt%) led to increased ye'elimite and C_3S dissolutions and accelerated ettringite formation in the first hours, while higher Li_2CO_3 contents led to a severe retarding effect on ye'elimite dissolution after the first 12 hours. Engbert and Plank [75] investigated the mechanism behind the accelerating effect of alginate and related biopolymers on the hydration of CA cement using *in-situ* XRD and complementary tests,

proposing that the alginate molecules provide a heterogeneous crystallization surface, favoring the first nucleation and growth of C-A-H phases and accelerating the hydration of CA cements.

Galan *et al.* [76] tested a new luminescent sensor technique for pH analysis to monitor the PC/slag, CSA and CA cement hydrations using *in-situ* XRD and isothermal calorimetry to correlate the hydration reactions with the changes in pH. For the PC-slag cement, a very high pH (> 13.0) was observed due to the dissolution of alkali sulfates, C_3S and C_3A, which provide significant amounts of hydroxyl and alkali ions to the solution. The CSA pastes presented a pH close to 11.0 at the first hours, which progressively increased with the dissolution of ye'elimite. Finally, the CA paste had a pH of 11.6, which, according to the authors, was mainly related to the early dissolution of monocalcium aluminate.

As for the effect of temperature on CA cement hydration, Goergens *et al.* [77] assessed the early hydration of CA-calcite mixes at 10, 23, 40, and 60°C using *in-situ* XRD. The temperature greatly influenced the CA cement hydration: the higher the temperature, the faster the clinker phases and calcite dissolution occurred. Consequently, the formation of the hydrate phases occurred faster at higher temperatures. At 23, 40, and 60°C, calcite dissolves during the CA main reaction, supplying carbonate for hemicarbonate and monocarbonate formation. However, at 10°C, these phases were not observed due to the very slow calcite dissolution, and the calcite acted as an inert filler.

2.1.5. Alkali-activated materials

Despite being less common than Portland and calcium (sulfo)aluminate cements, some studies used *in-situ* XRD to follow the reaction of alkali-activated materials. Sun and Vollpracht [78] studied the reaction of NaOH-activated fly ash, metakaolin, and slag at 20°C and 30°C using isothermal calorimetry and *in-situ* XRD. The authors observed that the amorphous solid precursors quickly dissolved within the first hours, and the amorphous gel (C-A-S-H/N-A-S-H) started to precipitate. After that, the dissolution rate of the precursors and the precipitation rate of the gels decreased smoothly with time. For the NaOH-activated slag, hydrotalcite was formed in the first hours in addition to C-A-S-H. The temperature rise from 20°C to 30°C increased the reaction rate for all systems, growing the content of amorphous precursors dissolved after 24 hours increased by 101.6%, 46.6%, and 52.4% for the fly ash, metakaolin, and slag systems, respectively. Firdous *et al.* 2021 [79] studied the reaction of calcium carbonate minerals in sodium silicate solution and its influence in alkali-activated systems using *in-situ* techniques (XRD and FTIR) besides TGA and SEM. The authors observed that calcite is dissolved in the first hours, resulting in an intense heat released; however, no crystalline product was formed during the first 5 hours of reaction. At approximately 6 hours, the heat release suddenly increases, related to the precipitation of natron ($Na_2CO_3 \cdot 10H_2O$), observed by *in-situ* XRD, and/or to the formation of poorly crystalline C-S-H, observed by *in-situ* FTIR. Gijbels *et al.* [80] evaluated the effect of incorporating phosphogypsum on the reactivity and hardened properties in alkali-activated slag matrix using *in-situ* XRD. The authors observed no gypsum, bassanite or anhydrite diffraction peaks, proving that the phosphogypsum was completely dissolved during the first minutes of reaction. Phosphogypsum incorporation also led to a fast formation of portlandite and

ettringite after the first hours; diffraction peaks of thenardite and merwinite were also observed in the first hours of reaction. After 22 hours, the sample consisted of a combination of amorphous hydration with thenardite and portlandite. However, it should be noted that the experimental conditions used by these authors were not appropriate, resulting in very low-intensity peaks (up to around 30 counts), resulting in poor XRD pattern quality, as further discussed next.

It is worth emphasizing that evaluating fresh alkali-activated samples through *in-situ* XRD can be challenging because they often require higher w/s ratios, reaching values of 0.7-0.8 [81–83]. This results in an increased diffuse contribution of free water (specifically, activating solution), potentially leading to QPA issues, as discussed in Section 4.2.

2.2. Experimental conditions

Table 1 summarizes the experimental conditions reported in the literature for *in-situ* XRD analyses of cementitious pastes. Different diffractometers were used for this purpose, such as X'Pert Pro (PANalytical), D8 Advance (Bruker), and D5000 (Siemens). However, other diffractometers can also be used as long as they provide adequate testing conditions, detailed next. The power operating conditions reported are within 30-40 mA and 40-45 kV. Reflection mode with Bragg-Brentano geometry is the most usual choice for fresh pastes (Figure 2a), but transmission mode may also be considered (Figure 2b); this will affect the choice for the sample holder. In this regard, Dalconi *et al.* [84] compared the use of Bragg-Brentano geometry with a 35 mm diameter sample holder covered with Kapton film, focusing transmission capillary with a boron-glass capillary with 0.5 mm internal diameter, and focusing transmission flat sample geometry with sample mounted between two Kapton foils for *in-situ* XRD measurements of fresh PC paste. The authors found that glass capillary shows a high background contribution up to 25° 2θ (CuKα) and requires high fluidity for proper casting, but it minimizes segregation and preferred orientation issues (discussed in Section 4). Bragg-Brentano geometry allowed fast sample preparation and good intensity at short counting times but was more susceptible to segregation and preferred orientation at the paste-film interface. Transmission flat sample measurements had the lowest experimental background contribution and low segregation; however, it induced strong preferred orientation and only allowed the use of a low sample amount (0.08 g, potentially not representative of the bulk paste) to avoid absorption problems.

Regarding reflection mode measurements, fresh samples should be poured into the sample holder and covered with a thin film to avoid water evaporation and sample carbonation. Kapton polyimide film (yellow foil in Figure 2a and Figure 3a) is the most used foil for this application, and its contribution to XRD patterns will be detailed in Section 3.2.1. Mylar PET foil can also be used for this purpose [75,85], but it is far less popular. As for the sample holder, little information is available in the literature; several works reported using "custom-made sample holder" but with no further information [39,44]. Figure 3a illustrates the sample holder used by Gobbo [86], disassembled (left) and loaded with fresh paste (right). Goergens *et al.* [77] used a fresh sample of 0.5 ml and 3 mm in thickness. In general, it should present an adequate area to ensure that enough X-ray radiation reaches the sample and sufficient depth to prevent radiation from reaching the bottom of the sample holder.

Regarding transmission mode measurements, fresh samples can be placed into glass capillary sample holders using a syringe (illustrated in Figure 3b) and sealed with wax, or mounted between two Kapton foils in a thin layer (~100 μm [87]) to minimize absorption effects.

A temperature control system is desired [24,41,47,49,73] since it avoids temperature increases due to continuous X-ray radiation [88,89] and dissipates the heat generated by the cement hydration. It is well known that a temperature increase enhances the reaction kinetics of both cement and SCMs [90,91]. Bach *et al.* [92] also observed that a temperature rise reduced the pH of the pore solution and increased the sulfate concentration through the ettringite dissolution/destabilization, besides affecting the Ca/Si ratio of C-(A)-S-H. The exact increase in sample temperature during a laboratory XRD test has not been reported yet. However, Ectors *et al.* [35] associated the differences between the hydration kinetics measured by isothermal calorimetry and *in-situ* XRD with such sample heating even when using a temperature control system; since it cooled the sample holder from the bottom surface, the top (measured) surface was not completely cooled. Thus, alternate measurement and rest intervals can also be applied, *e.g.*, recording a 10-minute scan every 30 minutes [31,93].

Copper radiation ($\lambda_{K\alpha1}$ = 1.54056; $\lambda_{K\alpha2}$ = 1.54439 Å) is the most common radiation for *in-situ* (laboratory) XRD. However, De la Torre and co-authors [94,95] successfully used molybdenum radiation ($\lambda_{K\alpha1}$ = 0.70930; $\lambda_{K\alpha2}$ = 0.71359 Å) for powder (laboratory) XRD analyses of cementitious materials. Recently, a combination of laboratory X-ray diffraction (using strictly monochromatic Mo$K\alpha_1$) and computed microtomography (μCT) showed that Mo radiation allows scanning thick capillaries (*e.g.*, 1 mm in diameter), ensuring accurate sample preparation without micro bleeding in paste [59]. Although it is not considered an *in-situ* study since the data collection time was too high (238 minutes), it was the first step to establishing a methodology to analyze unaltered samples and determine hydration mechanisms accurately with this setup.

In general, the collection time for *in-situ* laboratory XRD ranges between 10 and 15 minutes per scan. There seems to be a consensus that this is a reasonable time to assume that no significant change in sample composition occurred during each scan. High-speed detectors are required to enable such low collecting time while keeping good statistics, such as the X'Celerator (Panalytical) and LynxEye XE-T (Bruker) position-sensitive detectors, while point detectors should be avoided. Monochromators are interesting for powder diffraction since it removes $K\alpha_2$ radiation [96]. However, they significantly reduce the X-rays incidence in the sample, requiring longer collection times to reach good statistics (*e.g.*, >4 hours [59,97,98]), so it should be avoided for quick *in-situ* measurements. In turn, Ni filter (or similar) can be used to remove K_β radiation without significantly reducing the X-ray incidence.

Slits are used to collimate the X-ray beam and reduce axial divergence issues, but they also reduce the intensity of the diffraction peaks [99]. Thus, the set chosen must allow the equipment to apply enough radiation to provide reasonable intensity counts within the short period of *in-situ* analysis. In this regard, Rowles [100] recently investigated the effect of data quality and model parameters on Rietveld QPA results, concluding that a maximum intensity of at least 5000 counts

above background is desired in powder XRD for samples that contain minor/trace phases. This is close to that usually observed for *in-situ* XRD measurements in cementitious samples, with maximum intensities reaching around 3000-5000 counts [24,37,72,101]. Automatic slits are used for powder XRD measurements of cement samples [102], while to the best of our knowledge, the only report on using it for *in-situ* XRD of hydrating samples is from Raab and Pöllmann [93]. A systematic investigation of fixed vs. automatic slits for *in-situ* XRD measurements is required. Scan range is usually conducted from 5-8° 2θ to 40-55° 2θ (CuKα). Although powder XRD is often conducted up to 70° 2θ (CuKα), shortening the scan range allows for reducing the overall data collection time while keeping the main reflections of the major anhydrous phases: 11-44° 2θ for PC; 16-42° 2θ for CSA clinker; 11-50° 2θ for CAC and 8-55° 2θ for the calcium sulfate sources (for CuKα). Hydrated phases are formed during hydration, making it mandatory to start the measurements at lower angles. The starting angle mainly depends on the hydrated phases expected in the sample: while for pure ettringite binders, starting angles of 8° 2θ are reasonable, binders with AFm phases must be measured starting at lower angles. An example is the current research on alternative binders in which one major hydrate phase is strätlingite. Those samples must be measured from comparably low angles in as much as the (0 0 3) line appears at around 7° 2θ (CuKα). Besides, Jansen *et al.* [101] confirmed that no difference in the results was observed when working with 7-40° or 7-70° 2θ ranges (CuKα) for *in-situ* measurements of C_3S sample. Step sizes within 0.011-0.024° 2θ are generally used, which provide adequate resolution and agree with the values proposed by Rowles [100]. Finally, using a knife-edge (or beam knife) is also an interesting choice. Although it slightly reduces intensity counting, it significantly reduces low-angle air scattering, allowing a low-order background fitting polynomial in the refinement [103], as discussed in Section 3.

In summary, the experimental setup should acquire XRD patterns with the lowest background contribution and low-angle scattering possible within 10-15 minutes per scan, while maximum intensity counts of around 3000-5000 are desired.

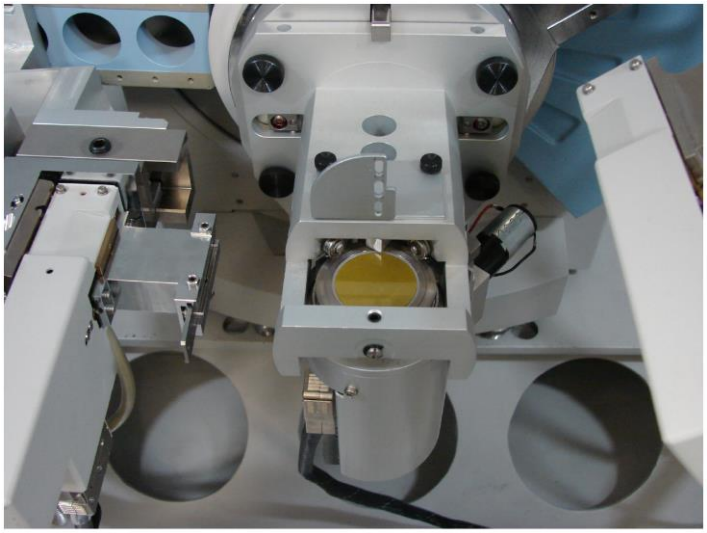

(a)

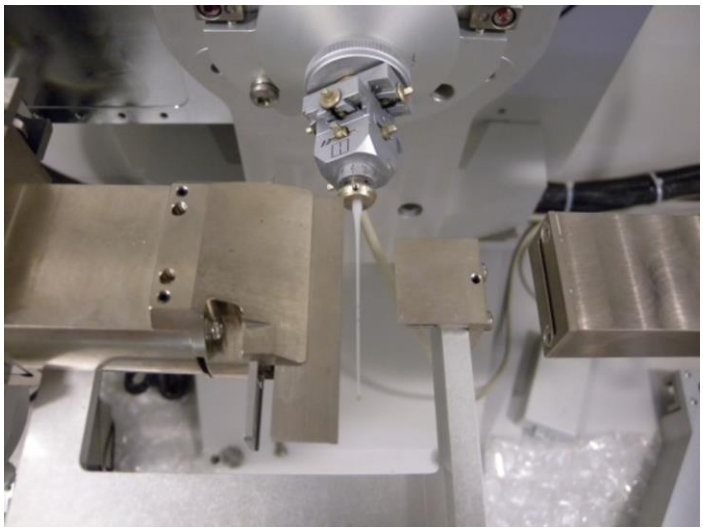

(b)

Figure 2. Geometries used for *in-situ* XRD measurements of fresh paste. (a) reflection mode with sample covered with Kapton film [86]; (b) transmission mode with capillary sample holder (courtesy of Luca Valentini).

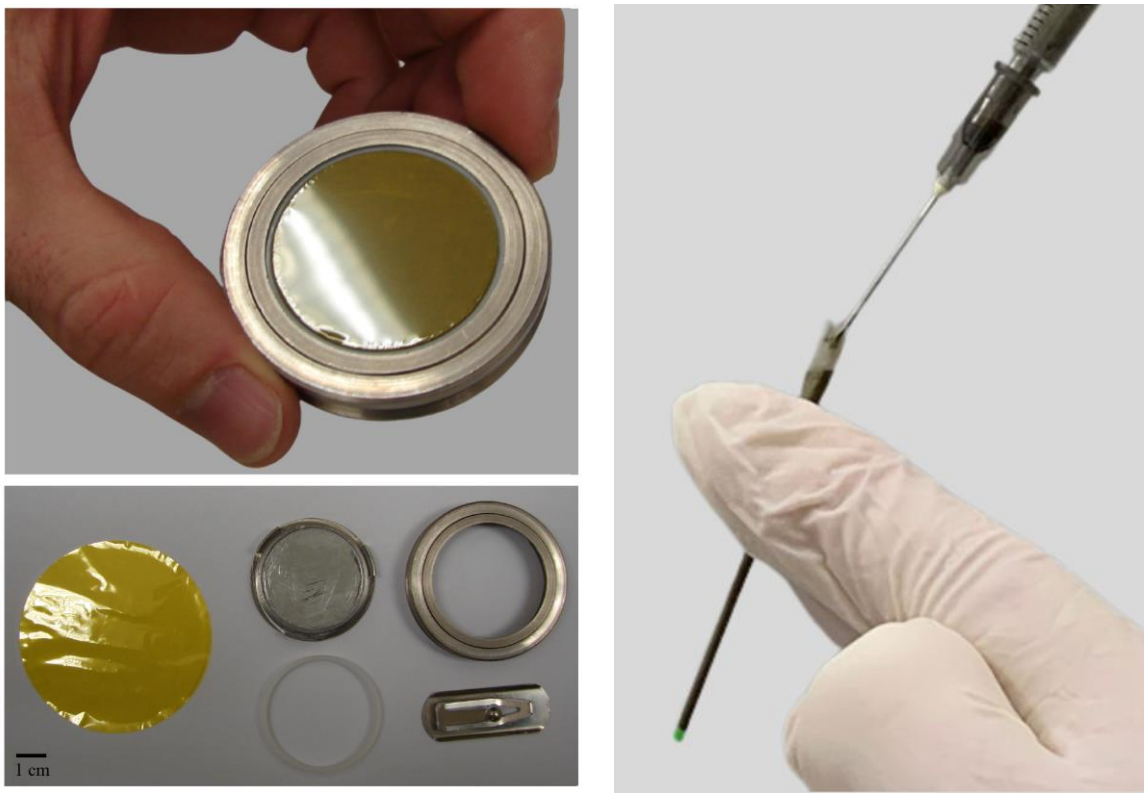

(a) (b)

Figure 3. Sample holders used for *in-situ* XRD measurements. (a) sample covered with Kapton film (adapted from [86]); (b) glass capillary filled with fresh paste.

466 Table 1. Experimental parameters used for *in-situ* XRD analyses reported in the literature.

Reference	Diffractometer	Detector	Radiation	Power	Angular range (°2θ)	Step size (°2θ)	Total time per scan (min)	Temperature control?	Sample analyzed
[24] [104]	Bruker D8	LynxEye	CuKα	40 kV; 40 mA	7 – 55	0.0236	10	Yes (23°C)	C_3S; w/s = 0.5
[105]	Bruker D8	LynxEye	-	40 kV; 40 mA	7 – 40	0.0236	15	Yes (23; 30; 37°C)	C_3S; w/s = 0.5
[101]	Bruker D8	LynxEye	CuKα	40 kV; 40 mA	7 – 40	0.0236	13.5	Yes (23; 37°C)	C_3S; w/s = 0.5
[44]	Bruker D8	LynxEye	CuKα	40 kV; 40 mA	7 – 40	0.0236	13.5	No	PC; w/s = 0.5
[45]	Bruker D8	LynxEye	CuKα	40 kV; 40 mA	7 – 40	0.0236	13.5	No	PC; w/s = 0.5
[65]	Bruker D8	LynxEye	CuKα (1)	40 kV; 40 mA	7 – 55	0.0236	-	Yes (20°C)	PC with and without PCE; w/s = 0.36
[22][(a)] [63][(b)]	PANalyticalX'Pert PRO(3)	PIXcel	CuKα (1),(2)	-	6 – 66[(a)]; 3 – 66[(b)];	0.026[(b)]	20	Yes (23°C)	[(a)]C_3S+gypsum; w/s = 0.5; [(b)]C_3S+PCE; w/s = 0.5
[41][(c)] [56][(d)]	PANalytical X'Pert PRO	-	CuKα (4)	45 kV; 40 mA	7 – 70	0.0167	14	Yes (20°C)	[(c)]C_3S + C_3A + gypsum; w/s = 0.5; [(d)]PC and LC^3; w/s = 0.4
[54]	PANalytical X'Pert PRO	X'Celerator	CuKα (1,5)	45 kV; 40 mA	7 – 55	0.0167	10	No	PC + SCMs paste; w/c = 0.4
[31][(e)] [37][(f)] [36][(g)]	PANalytical X'Pert PRO	X'Celerator	CuKα (1,5)	45 kV; 40 mA	7 – 55	0.0167	10	No	[(e)]C_3A + gypsum/hemihydrate; w/s = 1.0; [(f)]C_3S + C_3A + gypsum/hemihydrate; w/s = 0.5. [(g)]C_3S; w/s = 0.5.
[47]	PANalyticalX'Pert PRO	X'Celerator	CuKα	-	7 –70	0.0167	15	Yes (20°C)	White Portland cement; w/s = 0.4
[39]	Siemens D5000	SolX	CuKα	40 kV; 30 mA	7 – 41	0.024	15	Yes (23°C)	White Portland cement; w/s = 0.5
[50]	Bruker D8	LynxEye	-	40 kV; 40 mA	7 – 54.5	0.011	15	Yes (70 °C)	PC + lime + anhydrite; w/s = 0.8
[74]	Bruker D8	LynxEye	-	-	7 – 55	0.0236	10	Yes (23°C)	CSA + PC + anhydrite; w/s = 0.8
[46]	Bruker D8	LynxEye	-	-	–	-	10	Yes (23°C)	PC, w/s = 0.5 (6)
[77]	Bruker D8	LynxEye	CuKα (7)	40 kV; 40 mA	6 – 45	0.0236	7.4	Yes (10; 23; 30 °C)	CAC + calcite; w/s = 0.4 (6)
[78]	PANalyticalX'Pert PRO	-	CuKα (8)	40 kV; 40 mA	5 – 60	0.0167	14.3	No	NaOH-activated fly ash, metakaolin and slag; w/s = 0.4-0.8
[30]	PANalytical Empyrean	X'Celerator	-	-	5 – 55	-	-	No	C_3A+gypsum; w/s = 1.2
[29][(h)] [40] [(i)]	PANalytical X'Pert PRO	X'Celerator	CuKα	-	7 – 36	0.017	14	No	[(h)] C_3A+gypsum; w/s = 1.0 [(i)] C_3S+C_3A+gypsum; w/s = 0.4
[73]	PANalytical X'Pert PRO	X'Celerator	CuKα	40 kV; 40 mA	8 – 40	0.017	15	Yes (20°C)	C_3S + ye'elimite; w/s = 0.4
[60]	Bruker D8	LynxEye	CuKα	-	-	-	-	No	PC + PCE; w/c = 0.5
[49]	Bruker D8	LynxEye	CuKα	-	7 – 55	0.0236	10	Yes (20; 30 °C)	PC; w/c = 0.36
[69]	Bruker D8	LynxEye	CuKα	-	7 – 40	0.0236	10	Yes (23 °C)	PC + TEA; w/c = 0.41
[53]	Bruker D8	LynxEye	CuKα	40 kV; 40 mA	7 – 55	0.0236	14	No	PC + quartz/fly ash; w/s = 0.5

[35]	Bruker D8	LynxEye	CuKα [5]	40 kV; 40 mA	7 - 40	0.02	14	Yes (23 °C)	C_4AF + calcium sulfate + portlandite + calcite; w/s = 0.8
[67]	-	-	-	-	-	-	15	Yes (23 °C)	PC + polymers; w/c = 0.41
[66]	Bruker D8	-	CuKα	40 kV; 30 mA	8 – 44	-	-	No	PC + slag/calcined clay + C-S-H-PCE nanocomposite; w/c = 0.45 and 0.5
[75]	Bruker D8	VÅNTEC-1	CuKα [9]	40 kV; 30 mA	5 – 40	0.025	14	No	CAC + alginate; w/c = 0.5
[38]	Siemens D5000	SolX	CuKα	40 kV; 30 mA	7 – 41	0.024	15	Yes (23; 37 °C)	Synthetic cement; w/c = 0.5
[55]	Bruker D4 ENDEAVOR	LynxEye	CuKα	-	5 – 65	0.02	15	No	White Portland cement + nano-silica; w/s = 0.5
[68]	-	-	-	-	-	-	10	Yes (23 °C)	PC + polymers; w/c = 0.41
[33]	Rigaku SmartLab 9 kW-Advance	-	CuKα	-	5 - 36	0.02	1	No	C_3A; w/s = 1.0
[76]	PANalytical X'Pert PRO	-	CuKα	40 kV; 40 mA	7 - 55	0.017	-	No	PC, CSA, CA; w/c = 0.4-0.5
[48]	Bruker D8	-	CuKα	-	8 - 44	-	-	No	PC; w/c = 0.5
[79]	PANalytical Empyrean	-	CuKα	40 kV; 40 mA	12 - 56.8	0.0131	23.6	No	Alkali-activated limestone; w/s = 0.39
[80]	Bruker D2	-	CuKα	30 kV; 10 mA	6 - 55	0.02	13	No	Alkali-activated slag; activator/precursor ratio = 0.6
[106][j] [107][k]	PANalytical Empyrean	PIXcel^{1D}	$CuK\alpha_1$ [10]	40 kV; 40 mA	6 - 40	-	15	[h]Yes (25°C)	[j] LC^3 systems; w/s = 0.5. [k] Calcined phyllosilicates clinker-free systems.
[84]	PANalytical X'Pert PRO	PIXcel[3],[11],[12]	CuKα	-	2 - 66 [3]; 6 - 76 [11],[12]	-	15[11],[12] - 20[3]	Yes (23 °C)	PC; w/c = 0.5
[87]	PANalytical X'Pert PRO	X'Celerator[11],[12]	CuKα	45 kV; 40 mA	5 – 65	0.017	20	No	PC with and without calcium nitrite; w/c = 0.5
[93]	PANalytical X'Pert PRO	-	CuKα [13]	45 kV; 40 mA	5 - 70	-	10.42	No	$C_{12}A_7$; w/s = 2.0

[1] Ni filter; [2] Incident and diffracted beam optics included an elliptical focusing mirror, 0.04 rad Soller slits, divergence, and anti-scatter slits of 0.5° aperture; [3] Boron-glass capillaries with 0.5 mm internal diameter were used as sample holders; [4] 1° Soller slit; [5] full experimental setup available in the reference; [6] three replicates; [7] 0.3° divergence slit; [8] 0.5° divergence slit, 1° incident anti-scatter slit, 5.5° receiving anti-scatter slit; [9] 0.5º divergence slit; [10] Bragg–BrentanoHD monochromator; [11] equipped with a focusing elliptical mirror, measured at transmission mode; [12] sample mounted between two Kapton foils; [12] automatic slits. PC: ordinary Portland cement; CSA: calcium sulfoaluminate cement; CA: calcium aluminate cement; PCE: polycarboxylate-ether admixture; TAE: triethanolamine.

467

3. Data analysis

3.1. Background fit

The background fit is often overlooked, but it plays a crucial role in the accuracy of QPA. Manual background fitting should be avoided since it can affect the consistency of time-resolved analyses as well as increase the variability between different operators [108]. In addition, if not correctly fitted, the background can overlap the contribution of amorphous phases (*e.g.*, C-(A)-S-H and SCMs) and consequently underestimate their contents. In this regard, Stetsko *et al.* [102] demonstrated the importance of the background fit on the accuracy of QPA of Portland cements containing different SCMs. According to the authors, a 1st order Chebyshev polynomial + 1/2θ background fit is always concave upwards throughout the 7-70° 2θ range (CuKα) usually adopted for cementitious materials analyses. In turn, higher-order polynomials may lead to 2θ ranges that are concave downwards, overlapping the diffuse scattering contribution of the amorphous phases and consequently underestimating their contents. To overcome this issue, Bergold *et al.* [24] proposed that the experimental background can be incorporated into a phase model used in the refinement (for instance, into the Kapton film model), therefore allowing the use of a low-order background during refinement. However, one must be aware that the background reflects the sample chemistry to a significant extent through fluorescence scattering. Thus, at least a minimum background fit is necessary, *e.g.*, using a 1st order Chebyshev polynomial without 1/2θ term.

It is stressed that the background contribution in an XRD pattern is directly related to the experimental setup used. The use of a "disadvantageous" experimental setup can harm the analysis, for instance, resulting in strong low-angle scattering. This would require either the use of a high-order polynomial or a high starting angle. For example, Li *et al.* [109] quantified the presence of fly ash in hydrated pastes using powder and slice samples. The authors observed strong low-angle scattering, so the best XRD pattern fitting was obtained for the starting angle of 13.5° 2θ (CuKα). However, this starting angle excludes the main reflections of important phases such as gypsum, ettringite, and AFm.

3.2. Phase models

The refinement of *in-situ* XRD data deals with the simultaneous presence of amorphous contributions, *e.g.*, free water, Kapton film, C-(A)-S-H, and amorphous SCMs. These yield diffuse signals that increase the background. To systematically account for these contributions while achieving a good background fit, the development of phase models to describe these amorphous contributions is required. For example, Figure 4 shows an *in-situ* XRD pattern fitted with different phase models, where a 1st order Chebyshev polynomial was used, and a good fit (R_{wp} = 6.28%) was achieved. The strategies for the creation of these models will be discussed next. As for crystalline phases, a detailed list of the crystal structures used for XRD analysis of cementitious materials can be found in Ref. [108].

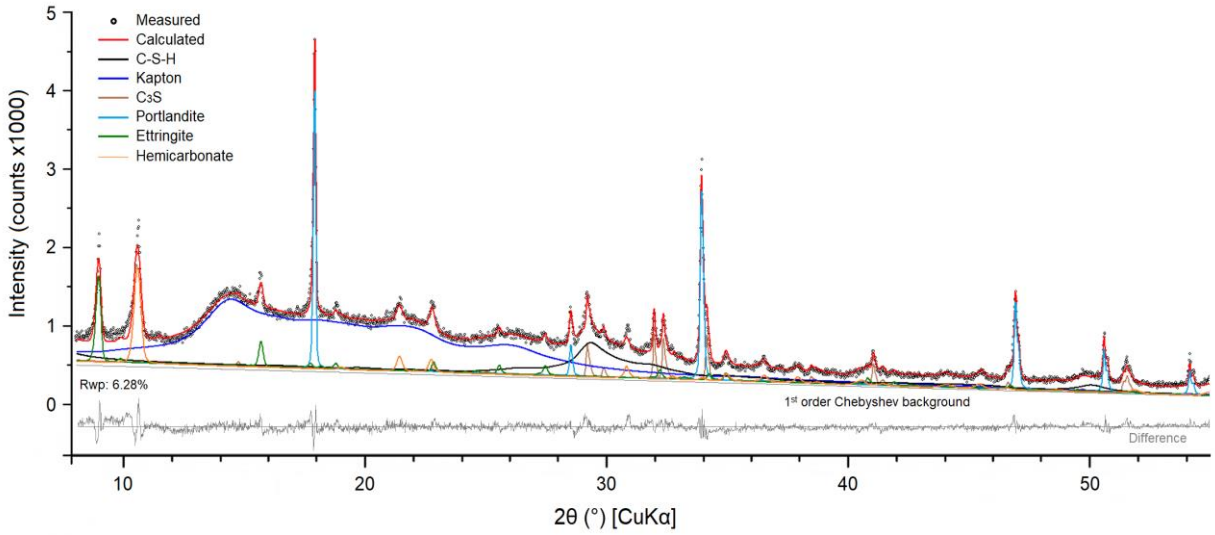

Figure 4. Example of fitted *in-situ* XRD pattern of C_3S-C_3A-gypsum paste at 48 hours of hydration (23 °C; w/s = 0.5). Reproduced from [37] with permission from Elsevier.

3.2.1. Kapton

The use of a thin film/foil to cover the sample is essential in time-resolved XRD experiments conducted in fresh cement paste due to two main reasons: (i) it prevents/reduces the water evaporation (discussed later in Section 4.3); and (ii) it prevents sample carbonation. The Kapton film (Figure 3a) is the most popular foil used for this purpose, which corresponds to a polyimide film of about 10 µm in thickness. Since it is composed of a thin polymer layer, the contribution of the Kapton film in an XRD pattern corresponds to a diffuse scattering within around 10-30° 2θ for CuKα radiation (Figure 5a).

In order to avoid manual background fitting and thus prevent the issues discussed in Section 3.1, a phase model can be used to account for the contribution of the Kapton film in an XRD pattern. Scherb *et al.* [110] detailed a procedure to create an *hkl* pseudo-phase to account for the Kapton contribution in addition to the experimental background. The authors adopted the space group *P4/mmm* and the lattice parameters a = 9.72 Å; c = 26.53 Å. A similar procedure was adopted by Andrade Neto *et al.* [31]. The procedure consists of creating and calibrating an *hkl* phase using a Pawley range to fit an XRD pattern of the Kapton film obtained experimentally. For this purpose, a standard crystalline material or a "zero diffraction" plate can be measured alone and covered with the Kapton film, isolating the foil's contribution, as reported by Maier et al [111] . For example, Figure 5a shows the XRD patterns of a silicon single-crystal zero background sample holder both without and with the Kapton foil measured under identical conditions. The difference in the XRD patterns can be attributed to the Kapton contribution and used to create the *hkl* phase. A similar approach was adopted by Hesse *et al.* [39]; however, these authors fitted the Kapton contribution with a specific set of peaks, *i.e.*, by creating a peaks phase. In addition, measuring the Kapton film over a standard crystalline

sample (*e.g.*, corundum in Figure 5b) allows to refine the lattice parameters of the Kapton *hkl* phase and therefore correctly place it along the 2θ axis [24].

It is stressed that creating and calibrating a model for each film used is essential since different thicknesses were reported in the literature (*e.g.*, from 7.5 to 25 µm [17,20,24,48,49]) and this can lead to differences in the Kapton contribution in an XRD pattern.

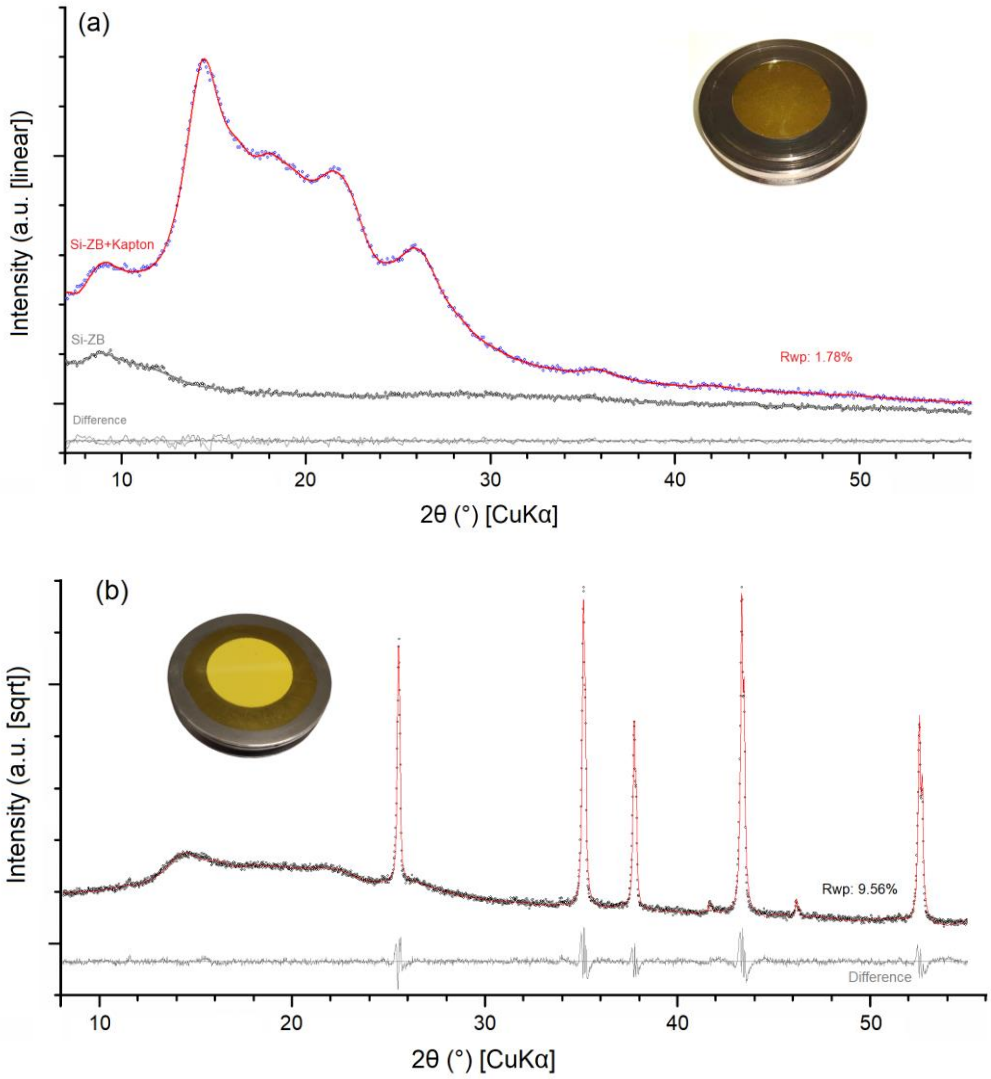

Figure 5. Samples covered with Kapton film for model creation. (a) silicon zero-background sample holder; (b) corundum sample. Data from [31].

3.2.2. Free water

The absence of structural order in the water makes its contribution in an XRD pattern diffuse. In contrast to cementitious powder samples, which are either anhydrous (for raw materials) or had the free water removed for hydration stoppage (for hydrated samples), fresh cement paste contains a significant portion of free water, especially within the first minutes/hours of hydration (*e.g.*, 1/3 of the weight fraction of a fresh paste with w/c ratio of 0.5). Thus, to accurately fit *in-situ* XRD patterns, the contribution of the free water must be considered [22]. Scherb *et al.* [110] described a routine for a

free water model creation, besides proposing the quantification of the free water content in a sample using the Partial or No Known Crystal Structures (PONKCS) method. The accuracy and detection limit of this quantification are discussed in Section 4.2. According to [110], to systematically account for the free water contribution, an *hkl* phase can be created using a similar procedure adopted for the Kapton film. Figure 6 presents the XRD patterns of a pure corundum sample covered with Kapton (in black) and a corundum:water mix in 50:50 wt% (in blue) measured under identical conditions. The difference between the two XRD patterns can be attributed to the free water. It is emphasized that such model is primarily used to account for the background increase caused by the free water, while its quantification is not mandatory (*e.g.*, by applying the PONKCS method), especially since the absolute weight fraction of the solid phases are commonly determined by the external standard method, making the determination of the free water content unnecessary.

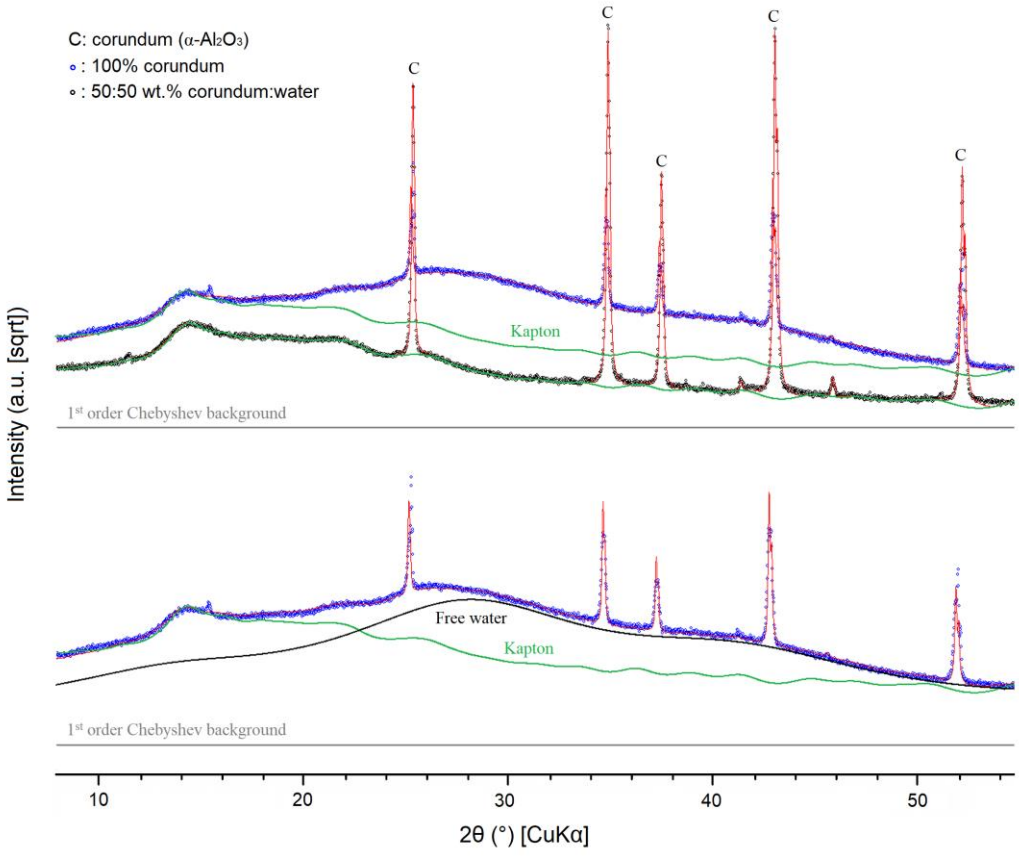

Figure 6. XRD patterns of pure corundum samples (black) and a corundum:water mix in 50:50 wt% (blue) for the creation of the free water model. Both samples were covered with Kapton film. Data from [31].

3.2.3. C-(A)-S-H

The fact that the amorphous/nanocrystalline structure of C-(A)-S-H yields a diffuse scattering signal in XRD is well known in the literature, and different approaches were used to describe its contribution in powder, slice, and fresh samples. Snellings and co-authors [103,109] created a C-S-H model based on a set of four pseudo-Voigt (PV) peaks obtained from a seven-year-old hydrated white

cement paste. Bergold *et al.* [24] created a *hkl* phase using a Pawley range to fit a fully-hydrated C_3S sample (containing only portlandite and C-S-H) with the crystal structure of 14 Å tobermorite (*F2dd* space group) from [112] as a starting point, obtaining the refined lattice parameters a = 11.81906 Å; b = 7.07097 Å; c = 58.92196 Å. This model can be seen in Figure 4. Similarly, Durdziński [113] used a one-year-old hydrated PC sample and the structure of 14 Å tobermorite to create a C-S-H model. Mejdi *et al.* [114] used the same 14 Å tobermorite structure and a six-month-old hydrated sample of silica fume and portlandite (1:3 ratio by weight) for the C-S-H model creation. However, Renaudin *et al.* [115] and Cuesta *et al.* [116] demonstrated that both the change in Ca/Si ratio and the presence of aluminum in C-(A)-S-H (for instance, by the incorporation of SCMs) change its structure and, therefore, its XRD signal. This suggests that a single C-S-H model may not be accurate to describe this phase generally.

It is stressed that the use of the PONKCS technique usually follows the quantification of C-S-H for *in-situ* samples. In hydrated PC (without SCMs) powder samples, it is reasonable to assume that the only amorphous phase present is C-S-H, so using either the internal or external standard methods directly provides the amorphous content in the sample, assumed as the C-S-H content. However, for fresh pastes and *in-situ* analyses, the presence of free water hinders this direct determination since it also yields an amorphous contribution (see Section 3.2.2). Thus, the previous calibration of the C-S-H model using a sample with known content is required. This allows the implementation of such model as a pseudo-phase in a Rietveld QPA routine, and this is the basis of the PONKCS method [117]. More details are given in Section 3.2.5. Alternatively, Valentini *et al.* [22] quantified the C-S-H formation in C_3S pastes through mass balance, based on the stoichiometry of the C_3S consumption measured by *in-situ* XRD. However, the authors alert that this approach may be suitable only for pure systems, while the presence of other phases in commercial PC prevents this approach.

3.2.4. Aluminate hydrates

Aluminate hydrates are of great interest especially concerning CSA, BYF, or CAC cement hydration. The challenge that arises from quantifying aluminate hydrate phases during *in-situ* XRD is that no structural models and, consequently, no entry in the ICSD database are available for some of the phases. While phases such as C_3AH_6, CAH_{10}, hemicarbonate, monocarbonate, and AH_3 can be quantified by Rietveld refinement based on the availability of accurate structural descriptions, phases like C_2AH_x (such as C_2AH_5, $C_2AH_{7.5}$, C_2AH_8, $C_2AH_{8.2}$) must be quantified mainly by adequate *hkl* phase models as for the C-S-H phase mentioned above. Goergens and co-authors quantified it by plotting the scale factor [77] and more recently by calibrating a phase model using the G-factor method [118].

The same issue also complicates the quantification of monosulfate phases with varying water content and C_4AH_{19}. Many of the phases which appear in cementitious systems do not have a full structural description, and hence it is not possible to give quantities by Rietveld refinement. Quantification could be done by a proper synthesis of such phases with a known amount, but it is still

challenging and needs more intense research [35,40]. An approximately accurate quantification of the different water-containing sulfate-AFm phases can be done based on the structure of monosulfate (kuzelite) [119] and the adjustment of the lattice parameter as a function of the water content in the interlayer [120,121], as seen in Figure 7 by plotting the *c* lattice parameter against the water content of sulfate-AFm phase (Figure 7a). Figure 7b shows the lattice parameter shift of monosulfate-12H towards monosulfate-14H and the respective fit by adjusting the lattice parameter in the monosulfate structure done in a cementitious system containing both monosulfate-12H and monosulfate-14H. Additional information on the hydration states of AFm phases can be found elsewhere [122]. We emphasize that although this approach has an interesting practical application, increasing the *c* lattice parameter would result in stretching all bonds in the crystal structure, which may not actually occur.

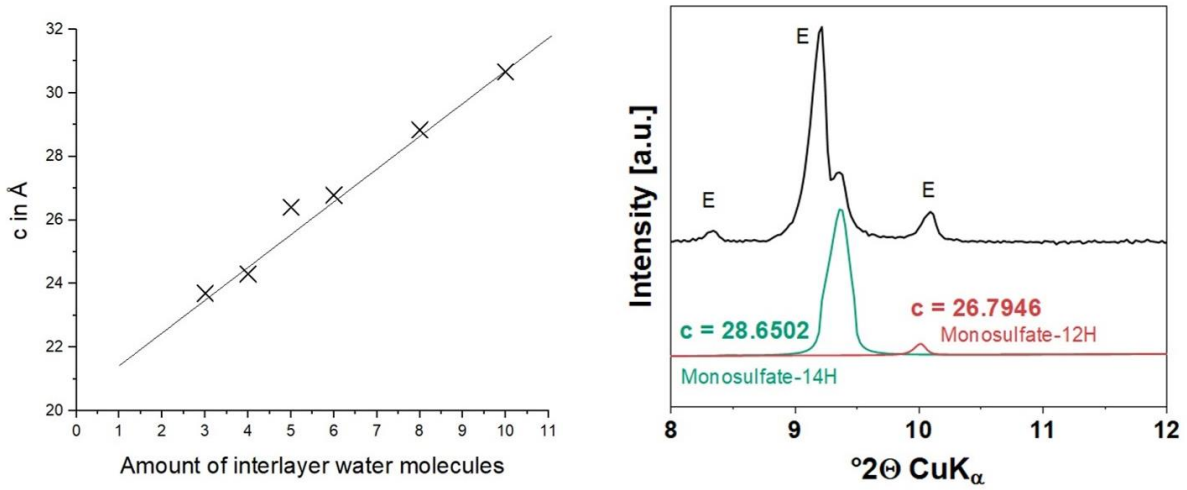

(a) (b)

Figure 7. Example of XRD analyses of AFm phases. (a) *c* lattice parameter vs. interlayer water content of sulfate-AFm (adapted from [121]); (b) lattice parameter shift of monosulfate-12H towards monosulfate-14H (unpublished data; courtesy of Irina Kirchberger).

However, the quantification of the AFm phases using *in-situ* XRD and Rietveld analysis has always the limitation that AFm phases often occur in a weakly crystalline state. This can lead to underestimating the quantities because the non-crystalline parts of the phases will not be quantified (see also Sections 4.2 and 4.5). The same holds true for the quantification of AH_3, which also often shows very low crystallinity. However, with an accurate description of the background as mentioned above (Kapton film, water), the detection and quantification of the phase can be done by applying *in-situ* XRD [72].

3.2.5. Amorphous supplementary cementitious materials

The use of amorphous SCMs in cement is increasingly common due to their environmental and technical advantages. The PONKCS method is often required to quantify these amorphous SCMs in a sample. In summary, this method creates a phase model to describe an amorphous contribution and then calibrates this model using a sample containing a known amount of such phase. This phase model can be composed of one or more peaks if no crystal structure information is available ("not

know"), or a pseudo-structure if some information is available ("partially know"), for instance, the space group and lattice parameters. After the model creation and calibration, it can be implemented in a Rietveld QPA routine.

Regarding the "not know" approach, Snellings *et al.* [103] used a single asymmetric split pseudo-Voigt (SPV) peak to model the amorphous fraction of metakaolin and a set of PV peaks to model the amorphous slag fraction. Similarly, Avet and Scrivener [123] used an SPV peak to fit the metakaolin fraction of calcined clays in addition to a second peak to fit the impurities of low-grade calcined clays (Figure 8a). Li *et al.* [109] also used an SPV peak to model the asymmetric profile of siliceous fly ash. Mejdi *et al.* [114] used a set of PV peaks to model the amorphous structure of glass powder. As for the "partially know" approach, Durdziński *et al.* [113] modeled the amorphous fractions of fly ash and slag using the crystal structure of anorthite ($P\bar{1}$ space group) and gehlenite ($P\bar{4}2m$ space group), respectively. Adu-Amankwah *et al.* [124] used the Pawley fit and the fundamental parameters approach [125] to model the amorphous fraction of slag but did not mention the space group adopted. Naber *et al.* [126] used the tetragonal structure of the *P4* space group to model the amorphous fraction of both silica fume (Figure 8b) and metakaolin. Stetsko *et al.* [102] used the space groups $Fm\bar{3}m$ and $Fd\bar{3}m$ to model the amorphous hump of slag and class F sly ash, respectively. The authors alerted that although the choice of the space group could be arbitrary, preference should be given to space groups that give only one peak within the region of the amorphous hump whenever possible.

In summary, both the "not know" and the "partially know" approaches for the PONKCS method usually yield good results, so the choice is up to the user. However, care must be taken for blended cements containing more than one amorphous SCM: de Matos *et al.* [127] found that XRD-PONKCS did not accurately distinguish the simultaneous presence of fly ash and calcined clay because their amorphous humps are closely placed along the 2θ axis.

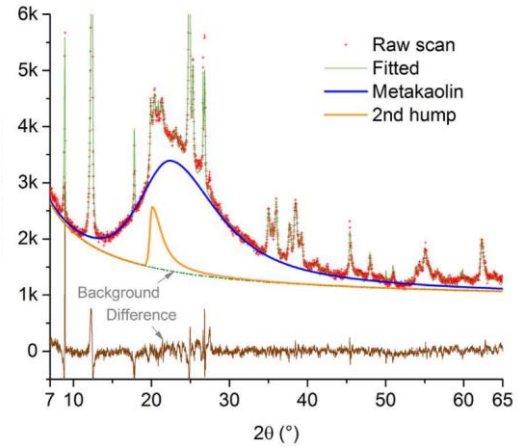

(a)

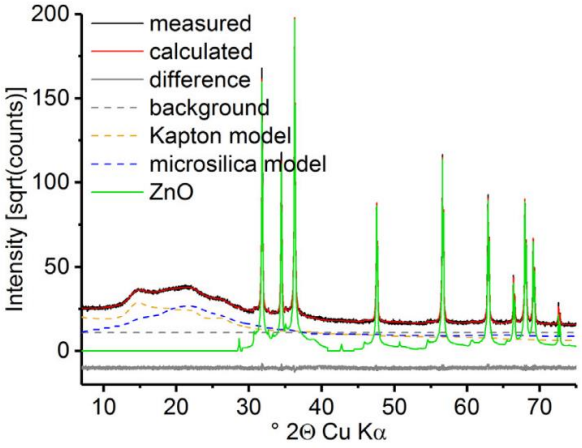

(b)

Figure 8. PONKCS models used for amorphous SCMs quantification. (a)"no know" approach for metakaolin [123]; (b)"partial know" for silica fume [126]. Reproduced with permission from Elsevier.

In future research, SCMs are getting more and more important. Besides the classical SCMs like fly ash, slag, natural pozzolans and clays, recycled cement stone will be added to the list [128]. This SCM, in turn, also shows a significant amount of amorphous, reactive silica-alumina-gel. The gel mentioned can be determined and quantified using the PONKCS method discussed above if the user consequently follows the guidelines of background description as given in this review. Figure 9 shows the specific description of the background and the description of a PONKCS phase in a mixture of alite and carbonated alite (containing calcite and amorphous silica gel).

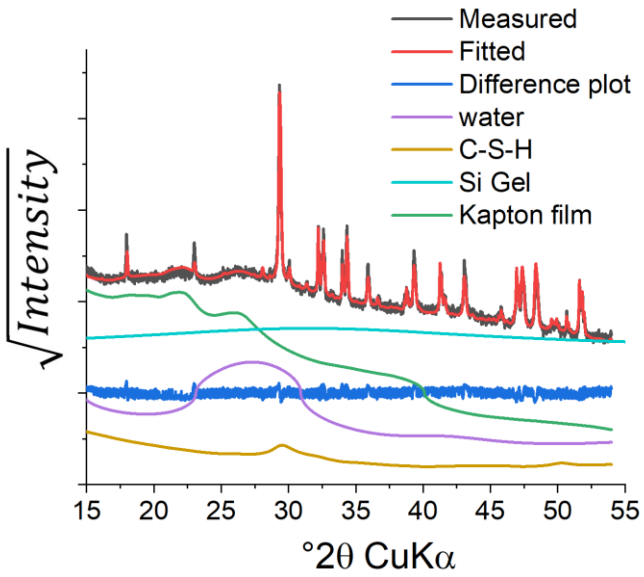

Figure 9. Fitted XRD pattern of alite + carbonated alite sample (unpublished data).

3.3. Qualitative and quantitative phase analysis

In-situ XRD measurement yields a set of patterns that can be analyzed from various viewpoints. The most straightforward strategy is a qualitative analysis, where the consumption or formation of phases is correlated with the increase or reduction of their peak intensities over time. For example, Figure 10 shows a set of XRD patterns obtained by *in-situ* analysis of a calcium sulfoaluminate paste reported by Galan *et al.* [76]. The hydration kinetics can be followed by the reductions in ye'elimite peaks and increases in ettringite and portlandite peaks over time.

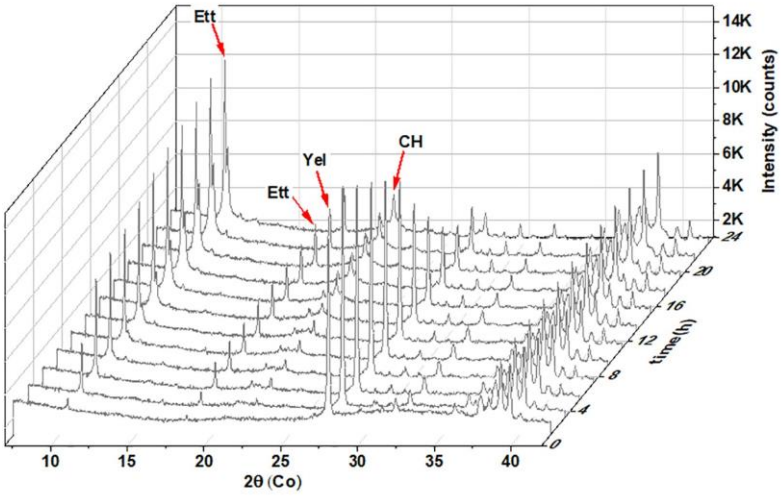

Figure 10. Example of qualitative *in-situ* XRD analysis of CSA paste (20 °C; w/s = 0.2). Ett: ettringite; Yel: ye'elimite; CH: portlandite. Reproduced from [76] with permission from Elsevier.

As a semi-quantitative strategy, intensity counting approaches can be performed. Padilla-Encinas *et al.* [129] used *in-situ* XRD with intensity counting analysis based on the peak with the highest intensity for each phase to evaluate the early hydration of calcium sulfoaluminate clinker. Quennoz and Scrivener [29,40] evaluated the area of a single representative peak for each phase over time for C_3A-gypsum pastes. Steger *et al.* [130] used intensity counts over time to evaluate the formation of aluminate phases in cements containing 70 wt% clinker replacement with slag. However, these approaches rely on the intensity/area of a single peak for each phase, while preferred orientation can occur especially for flat or elongated crystals (*e.g.*, portlandite and gypsum), leading to inaccurate results and interpretations (see Section 4.4). Furthermore, many factors can affect the background contribution, and some of these contributions vary over time (*e.g.*, free water, C-(A)-S-H, and amorphous SCMs). By considering absolute intensity values, these background contributions are disregarded. Therefore, care must be taken when conclusions are based on intensity counting analyses. Alternatively, Kirchheim *et al.* [30] used the reference intensity ratio (RIR) [131,132] to evaluate the content of each crystalline phase over time in C_3A-gypsum pastes. This method compares the intensity of one or more peaks of a determined phase with the intensity of a standard material to obtain an approximate phase content and was previously used for powder XRD in cementitious samples [133].

The determination of the weight fraction of each phase (*i.e.*, QPA) is in most cases desired, but the presence of poorly crystalline phases may prevent it, as discussed later in Section 4.5. Nonetheless, the scale factor of these phases can be used to indirectly evaluate their content over time. While the intensity counting approach relies on a single peak of the XRD pattern, the scale factor of a phase accounts for its contribution in the whole pattern, therefore minimizing preferred orientation issues.

For quantitative analysis, the Rietveld method is the most popular approach. This method assumes that all the phases in the sample are known, and all the phases are crystalline, yielding a relative weight fraction of each phase normalized to 100%. However, the presence of different

amorphous contributions in hydrating cementitious samples, in addition to the fact that the total fraction of the crystalline phases varies in time, makes the direct use of the Rietveld method inaccurate [22]. Thus, it is crucial to determine each phase's actual content (*i.e.*, their absolute weight fraction). The use of the internal standard method requires the incorporation of a standard material in the sample. This approach was used by Sun and Vollpracht [78] for *in-situ* XRD investigations of NaOH-activated fly ash, metakaolin, and slag samples. However, adding such standard material in the system can affect the hydration kinetics due to its physical effect (the so-called filler effect) [134]. Thus, the most suitable strategy is the use of the external standard method. This approach was first proposed by O'Connor and Raven [135] and was remastered by Jansen *et al.* [44,136], which refers to as "G-factor approach". It consists of measuring a standard sample (with high purity and crystallinity degree) using the same testing conditions adopted for the "target" sample to calibrate the G-factor given by Eq. 1. The absolute weight fraction of each phase in the target sample is then calculated using Eq. 2. The mass absorption coefficient (MAC) values of the samples are calculated from their chemical compositions. In the case of *in-situ* analyses where the fresh paste is covered with Kapton, the external standard material must also be covered with the Kapton film to avoid differences in X-rays absorption between the sample analyzed and the standard material [44].

$$G = S_s \frac{\rho_s V_s^2 \mu_s}{W_s} \quad (1)$$

$$W_i = S_i \frac{\rho_i V_i^2}{G} \mu^* \quad (2)$$

where W is the weight fraction of the phase (i) or the standard (s), in wt%; S is the refined scale factor of the phase (i) or the standard (s); ρ is the density of the phase (i) or the standard (s), V is the unit cell volume of the phase (i) or the standard (s) in Å^3; and μ is the MAC of the sample (*) or the standard (s), in cm^2/g.

3.4. Refinement strategies

In-situ XRD analysis deals with dozens of patterns for each sample, and each of these may contain several phases. Therefore, an adequate data analysis (or refinement) routine is essential to improve the consistency of this time-resolved studies, besides avoiding drifting and unrealistic results. At first, any software capable of conducting Rietveld analysis can be used for QPA of *in-situ* samples. For instance, Zunino and Scrivener [41], Scherb *et al.* [107], and Ma *et al.* [73] used the HighScore Plus (PANalytical) software to conduct the QPA of *in-situ* laboratory XRD samples. Álvarez-Pinazo *et al.* [17] used GSAS to conduct the QPA of *in-situ* synchrotron XRD of sulfobelitic cements. Maier *et al.* [106] used Profex-BGMN to evaluate laboratory *in-situ* XRD data for LC^3 systems. However, most software only refine individual XRD patterns, making the QPA very time-consuming. Besides, the same refinement routine must be applied to all the patterns for the reasons mentioned above. Thus, software that allow the refinement of multiple XRD patterns simultaneously – for instance, TOPAS

(Bruker) [137] – can increase the speed and consistency of the analysis and may be preferred [15,35,65,72,77,138,37,39,44,45,49,50,54,60].

Regarding the parameters refined in the Rietveld analysis, the "sample displacement" or "sample shift" parameter is the first to be mentioned. Figure 11 shows a set of *in-situ* XRD patterns obtained for a C_3S-C_3A-gypsum hydrating paste from [37]; the scans were recorded every 30 minutes up to 48 hours, totaling 96 patterns. One can note a constant background contribution from the Kapton film, in addition to two general shifts over time: the patterns shifted along the 2θ axis due to the sample displacement (discussed next) and downwards due to the reduction of free water (by the formation of hydrated phases). Regarding the sample displacement, Figure 12 shows the relative scale factor of the crystalline phases of a cubic C_3A-gypsum paste up to 48 hours of hydration, in addition to a picture of the sample after 48 hours from [37]. One can note that the sample displacement grows until the end of the ettringite formation, which caused the expansion of the sample and evidence that the refinement of the "sample displacement" parameter is essential. It is important to mention that refining the "zero error" parameter, which accounts for a misalignment of the goniometer, leads to a similar practical result than refining the sample displacement parameter, *i.e.*, corrects the 2θ pattern shift. However, the sample displacement and the zero error should not be refined together, so it is crucial to have a calibrated equipment.

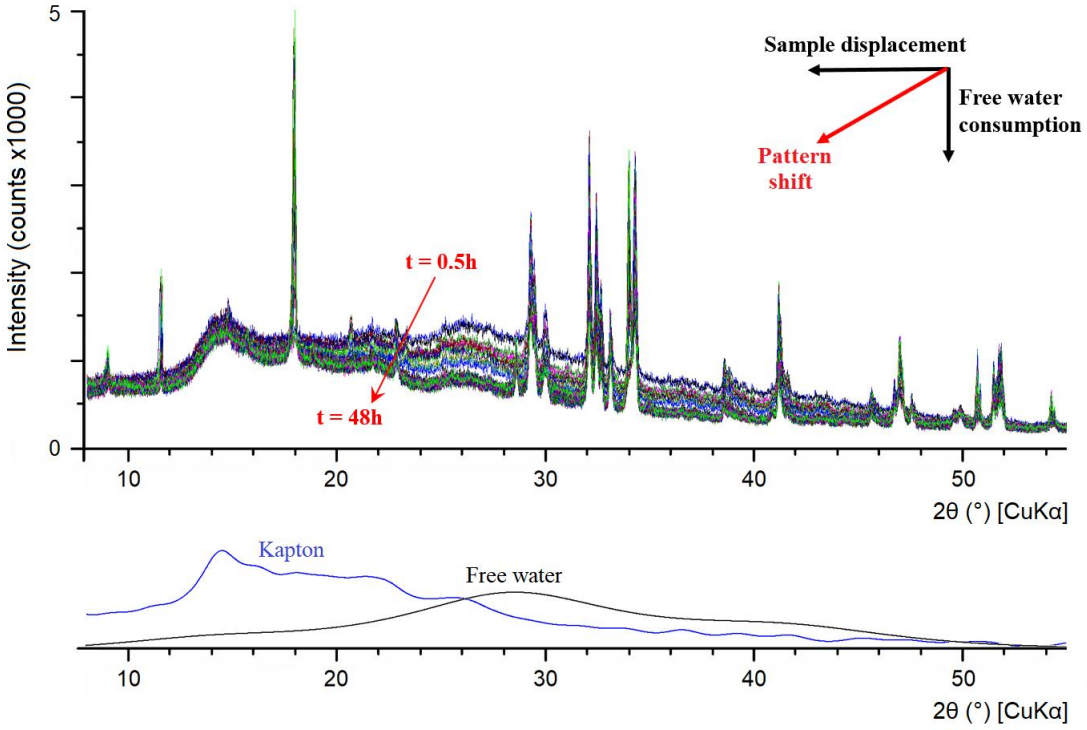

Figure 11. Example of a set of *in-situ* XRD patterns for a C_3S-C_3A-gypsum paste during the first 48 hours of hydration (w/s = 0.50; 23 °C). Data from [37].

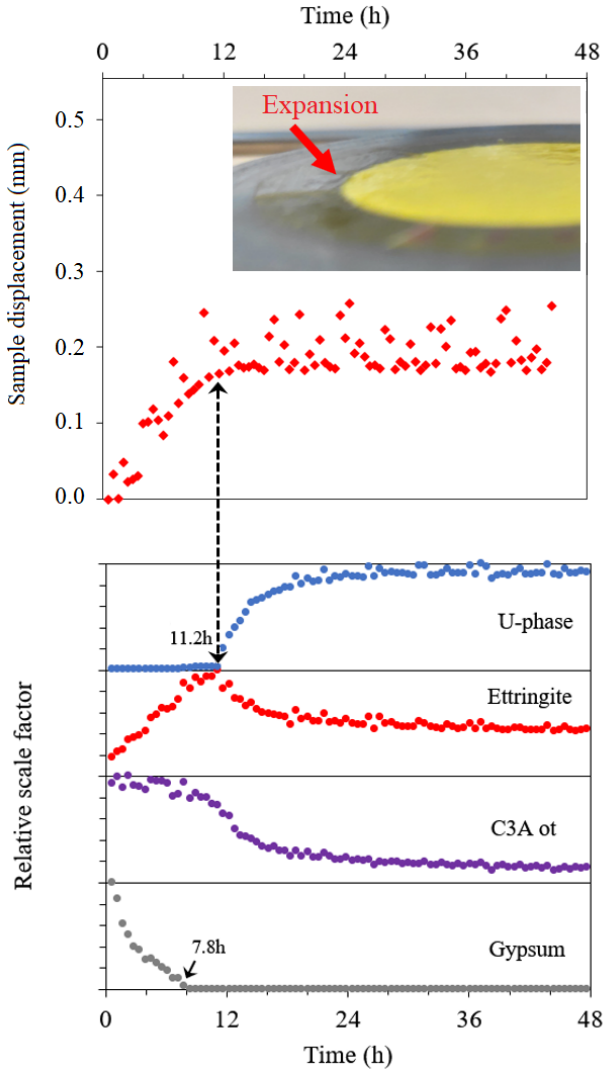

Figure 12. *In-situ* XRD of hydrating C_3A-gypsum paste (w/s = 1.0; 23 °C): relative scale factor of the phases and sample displacement over time, in addition to a picture of the sample after 48 hours. Adapted from [31] with permission from Elsevier.

The background fit is another global parameter to be refined in the Rietveld analysis of *in-situ* samples. The importance of using a proper background fit was discussed in Section 3.1. A good strategy is to account for the experimental background in one of the phase models present in all the samples; the Kapton model is a good candidate for this. Nevertheless, the experimental background cannot be fully described this way since it also depends on sample chemistry, so a background fit is still required – see Section 3.1. In addition, the scale factor of the Kapton model can be refined in an external standard sample covered with the film and measured just before the experiments and then be fixed for the hydrating samples. Since the instrumental background and the Kapton contribution should remain constant during the experiment, this reduces the chances of unrealistic background variations during the refinement [24] besides reducing the number of variables refined in hydrating samples. Moreover, graphically checking the Kapton signal in XRD – even during the experiment – may provide a general idea of data collection quality. If the Kapton signal is far above or below the expected (*e.g.*, in comparison with the standard sample), there was probably some experimental error.

Regarding the (micro)structural parameters of the phases, the lattice parameters of the anhydrous phases should be refined in dry samples and fixed for hydrated samples as we assume that no significant crystal expansion/shrinkage occurs during the first hours/days of hydration [22,108]. Microstrain can also be refined in dry samples and fixed for hydrated samples since it does not significantly change over time [39]. Atomic displacement or thermal parameter (B_{iso}) should only be refined in dry samples with high-quality data collection; otherwise, the values from the original crystallographic information files (CIF) should be kept [139]. In turn, the crystal growth kinetics may require the refinement of the lattice parameters over time for hydrated phases. For instance, Snellings *et al.* [15] and Merlini *et al.* [20] respectively observed the variation of the lattice parameters of portlandite and ettringite within the first 6-8 hours of hydration through *in-situ* synchrotron XRD. Peak shape modeling over time – for instance, by refining the crystallite size through the fundamental parameters approach [125] – can be necessary, especially for hydrated phases [15,24,39]. Finally, accurately distinguishing the C_3S and C_2S polymorphs and determining their proportions may not be easy, even in anhydrous cement, due to the high degree of overlap between their XRD patterns. In this sense, the correlation matrix allows for checking to what extent two parameters are related, enabling to avoid separately adjusting highly correlated parameters [13,140].

It is important to remember that most software used for Rietveld refinement are least-squares systems [137] that will seek the best curve fit within the constraints imposed on it. In other words, the software will yield the combination that gives the lowest "weighted profile R-factor" (R_{wp}) and "goodness of fit" (GOF) values possible even if the results have no physical meaning, *e.g.*, by excessively reducing the crystallite size of a phase or considering phases that are not likely to be in the sample. To avoid unrealistic peaks shifting and/or broadening, one can constrain the lattice parameters variation (to ±1% from the original CIF values) and the crystallite size value (usually within 50-1000 nm) during refinement. Therefore, it is essential to visually check the Rietveld fit by graphically comparing the observed (measured) and calculated (proposed) patterns and ensuring that the proposed model is chemically plausible [141]. In view of that, independent techniques to support the *in-situ* XRD results are recommended, as discussed later in Section 5.

In summary, some recommendations related to the refinement strategy of *in-situ* XRD data are drawn:

- The least number of variables possible should be refined to obtain a good (and physically coherent) adjustment. This avoids unrealistic results and the chance of drifting;
- The sample displacement parameter must be refined due to sample expansion/shrinkage during hydration;
- A background fit with the lowest terms possible should be used (see Section 3.1). Manual background fitting should be avoided. Including the instrumental background in the Kapton model, besides refining its scale factor in an external standard sample and fixing it for hydrating samples is a good strategy to avoid unrealistic background fit;

- The lattice parameters of the anhydrous phases should be refined in dry samples and then fixed. Hydrated phases may require the refinement of (micro)structural parameters over time. Lattice parameters and crystallite size variations may be constrained to avoid unrealistic values;
- It is crucial to visually check the curve fit and graphically compare the observed vs. calculated patterns, ensuring that the latter is chemically plausible.

4. Advantages and limitations

4.1. Phase preservation

Although the sample preparation for *ex-situ* XRD analysis is not in the scope of this paper, a brief introduction to the topic is required; for further information, the reader may refer to [142]. XRD analyses of hardened cementitious pastes are often conducted in powder or slice samples which usually require hydration stoppage and sample preparation procedures that affect the microstructure of some phases [108]. For hydration stoppage, different techniques are available such as direct drying (*e.g.*, vacuum or freeze-drying) and solvent exchange (*e.g.*, using acetone, diethyl ether, or isopropanol). Since direct drying is more aggressive to paste's microstructure [143], the use of solvent exchange methods (especially isopropanol) is currently recommended in most cases [144]. However, even for the most gentle hydration stoppage procedures, phases containing high water content (*e.g.*, ettringite and AFm) can partially decompose [108]. As for sample preparation, the slice cutting step can deteriorate the structure of fragile phases besides leaching them if conducted with water as cooling agent [14,145]. Thus, a low-speed cutting procedure with isopropanol as cooling agent may be preferred [126]. For powder samples, the grinding procedure can dehydrate some phases if conducted by high-energy grinding [142]. Therefore, more gentle grinding procedures are preferred, such as hand-grinding the sample in an agate mortar [98,138] or using a specific mill for XRD sample preparation (*e.g.*, McCrone micronizing mill) with a cooling agent [146]. Schreiner *et al.* [50] compared these two grinding procedures, observing that McCrone mill yielded more reproducible results than hand grinding. Nonetheless, ground samples tend to face ettringite and AFm deterioration [108]. In summary, hydration stoppage and sample preparation procedures will hardly prevent the deterioration of fragile phases.

In this context, *in-situ* XRD avoids hydration stoppage and additional sample preparation procedures, preventing phase damage. Figure 13 shows an example of the same PC paste at 24 hours of hydration, measured both at powder and fresh paste forms. For the powder sample, hydration was stopped by solvent exchange following [144] and ground in agate mortar until passing through a 45 µm-opening mash. The samples were measured under the same testing conditions, except for the total counting time of 10 minutes for the fresh sample and 30 minutes for the powder sample. Despite the lower data acquisition time for the fresh sample, which resulted in lower C_3S and portlandite peak intensities, the higher intensity of 9.1 and 16.5° 2θ (CuKα) ettringite peaks is evident. The same trend was observed by Ma *et al.* [73] and Redondo-Soto *et al.* [57] (see Figure 21) when comparing *in-situ* and *ex-situ* (powder) XRD. Balonis *et al.* [85] used wet samples covered with Mylar foil to evaluate

chloride- and hydroxy-AFm's and preserve their water contents for punctual (*i.e.*, not time-resolved) data collection. Alternatively, Naber *et al.* [126] used time-resolved XRD to follow the reaction of silica fume and metakaolin in PC pastes up to 112 days. The authors used hardened slice samples covered with Kapton film to prevent sample carbonation and account for the experimental contribution in the pattern fit.

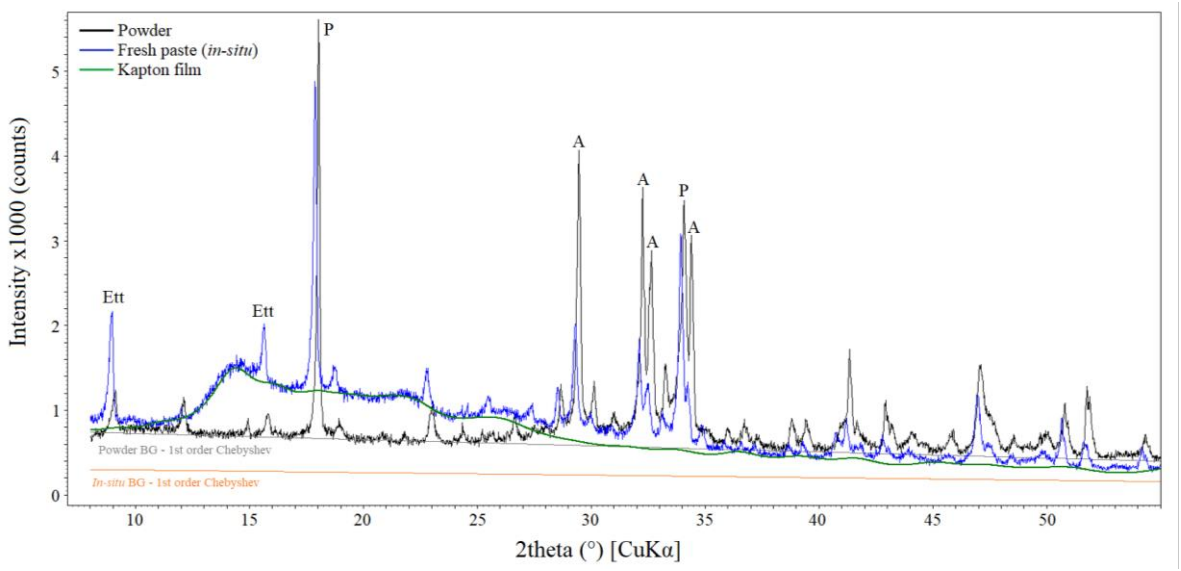

Figure 13. PC paste at 24 hours of hydration (w/c = 0.4; 23 °C) measured at the powder form (*ex-situ*) and fresh paste (*in-situ*). Ett: ettringite; A: alite (C_3S); P: portlandite. Adapted from [145] with permission from Elsevier.

4.2. Precision and detection limit

Precision can be assessed by determining the closeness of agreement among test results obtained under prescribed conditions [147], while accuracy refers to how close a result is to the "true value". For PC composition measurements, accuracy cannot be determined since its "true value" is not exactly known and can only be well-estimated and supported by complementary techniques. For instance, García-Maté *et al.* [97] used a state-of-the-art powder laboratory and synchrotron XRD set to confirm that the standard Portland clinker SRM 2686a certified by NIST [148] had an overestimated C_2S content.

In Portland and calcium (sulfo)aluminate cementitious samples, the major crystalline phases are usually C_3S, C_2S, and ye'elimite from anhydrous cement, besides ettringite and portlandite for hydrated pastes. These phases are often present in anhydrous commercial cements in contents of around 15-70 wt%, besides up to ~100 wt% in synthetic systems. Due to the high content of these phases, in addition to the existence of well-defined crystal structures, the quantification of their content usually does not bring significant problems and yields good results for *in-situ* analyses. However, it is worth emphasizing that C_2S correct modeling and quantification may be tricky due to its high peak overlap with C_3S, as mentioned in Section 3.4 and reported by Ref. [97]. For instance, Figure 14 shows the absolute C_3S content over time in four independent PC samples obtained by *in-situ* XRD reported by Jansen *et al.* [44]; variations of up to ±2 wt% were observed. Similarly, Goergens [77] reported

standard deviation values of 2-3 wt% for monocarbonate and CAH_{10} (both with >15-20 wt%) for three independent *in-situ* XRD measurements of calcium aluminate cement hydrating pastes. These are consistent with inter-lab deviation values reported in the literature for powder XRD of cementitious materials [13,95,149–151].

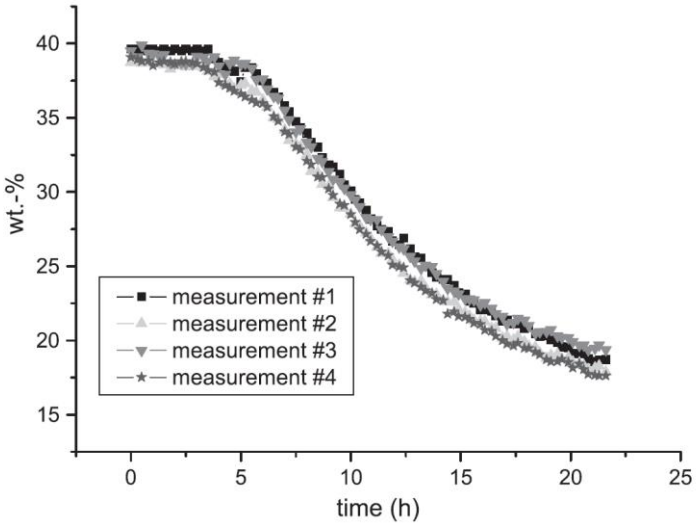

Figure 14. C_3S content during hydration of PC for four *in-situ* XRD independent measurements (23 °C; w/s = 0.5). Reproduced from [44] with permission from Elsevier.

Minor phases are also found in anhydrous and hydrated PC samples, which can derive from the clinker (*e.g.*, C_3A, C_4AF, and alkali sulfates), calcium sulfate (gypsum, bassanite, anhydrite, etc.), impurities/undesired phases (*e.g.*, periclase and free lime), or from the hydration reactions (*e.g.*, AFm's). In addition to their low content (often below 5 wt% of dry cement), some of these phases quickly dissolve in contact with water (as in the case C_3A, gypsum, and alkali sulfates) [44] or are hydrated (*e.g.*, bassanite) [31,65], so the content observed at the first measurement is usually very low. Besides, some of these phases can face preferred orientation issues (see Section 4.4) and/or present poor crystallinity (see Section 4.5), which make their quantification even harder. In this case, the use of complementary techniques to support the *in-situ* XRD data is advised, as discussed in Section 5. Figure 15 presents the phase content over time of some minor phases in PC pastes determined by *in-situ* XRD. Figure 15a from Jansen *et al.* [44] shows a reduction of about 2 wt% in the absolute C_3A content (relative reduction of 28%) at the first measurement compared to the content expected from the dry cement. In addition, the authors reported the absence of bassanite and arcanite at the first *in-situ* measurement, even though these phases were detected in the anhydrous cement (1.5 wt% and 0.9 wt%, respectively). Pott *et al.* [65] and Andrade Neto *et al.* [31] also reported the absence of bassanite in the first *in-situ* XRD measurement (at 10-30 minutes of hydration) despite the presence of this phase in the anhydrous samples. Figure 15b shows the anhydrite content over time of PC pastes with quartz and fly ash additions reported by Dittrich *et al.* [53]. The authors' determination limit and standard deviation values were 0.3 wt% and 0.5 wt%, respectively. Despite this relatively low deviation, it is difficult to identify a significant difference between samples over time. Finally, there are no reports on round robin tests to assess the reproducibility (*i.e.*, between-laboratory variability) of *in-situ*

laboratory XRD measurements in hydrating cement samples, in contrast to powder XRD of anhydrous and hydrated cement samples [150–152].

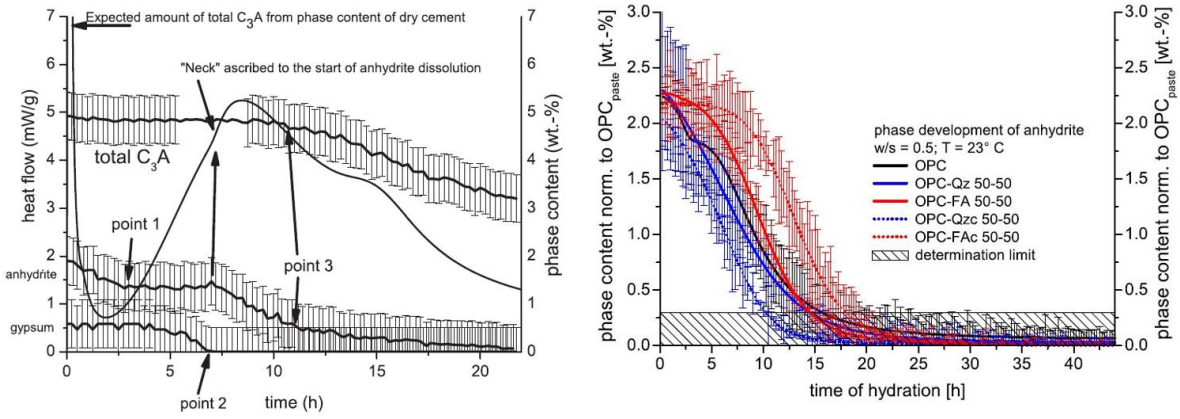

(a) (b)

Figure 15. Phase content of minor phases determined by *in-situ* XRD. (a) C_3A, anhydrite and gypsum in PC paste (23 °C and w/s = 0.5) [44]; (b) anhydrite in PC containing quartz [Qz] and fly ash [FA] (23°C and w/s = 0.5) [53]. Note: the hatched area in (b) represents the determination limit. Reproduced with permission from Elsevier.

Another "phase" present in fresh cementitious samples is free water. Scherb *et al.* [110] proposed quantifying the free water content in different powder-water mixes through XRD-PONKCS analysis. Figure 16 shows the correlation between the water content measured and the actual w/s ratio of the samples, besides their theoretical water contents. The authors observed that: (i) for a stiffened condition (*i.e.*, low water content), the scattering contribution of the free water on XRD pattern was constant and hardly detected; (ii) when the water content was increased beyond the point that the sample reached a paste consistency, there was a correlation between the increase of the scattering contribution of free water in XRD and the water content added; and (iii) when an excessive content of water was added, particle sedimentation occurred and the water segregates on the sample surface, so the contribution of the free water significantly increased. In addition, segregation would lead to a locally higher w/s ratio (*i.e.*, higher water availability), affecting the hydration and thus leading to biased results. In this scenario, segregation may be avoided by using transmission mode with flat samples or thin capillaries with continuous spinning [84]. Besides, Figure 16 shows that the accuracy of this quantification depends on the solid particles in the system: while fly ash and limestone yielded good prediction results, metakaolin and metamuscovite led to significant errors for w/s ratios above 0.4. Thus, the accuracy of this analysis depends not only on the water-to-solid ratio but also on the type of solid particles. Andrade Neto *et al.* [31] reported an excessive water contribution in XRD patterns of cubic C_3A-gypsum paste with a w/s ratio of 1.0 within the first 8 hours of hydration, which prevented proper phase analysis in this period, while this issue was not observed for orthorhombic C_3A paste (more reactive) with gypsum, or either C_3A with bassanite.

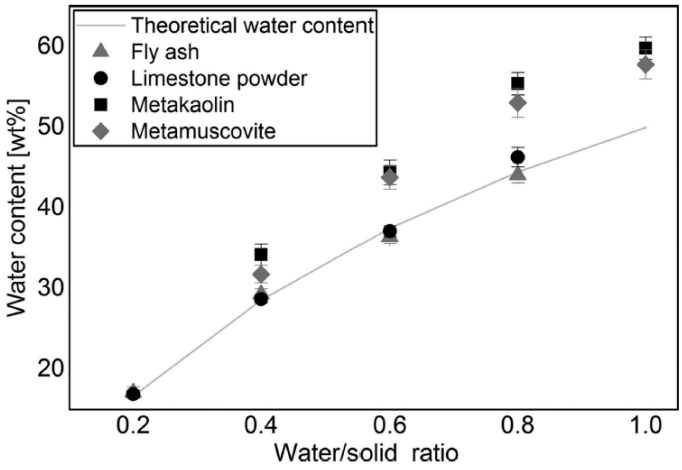

Figure 16. Quantification of the free water content by XRD-PONKCS. Reproduced from [110] with permission of the International Union of Crystallography.

An alternative to estimating the free water content in fresh samples is by determining the water consumed by the formation of the hydrated phase through stoichiometric calculations. Figure 17 exemplifies it, where Jansen *et al.* [46] determined the water consumed by the ettringite, portlandite, and C-S-H formation in white Portland cement paste from their contents measured by *in-situ* XRD, observing a good agreement with the free water content determined by ^{1}H NMR. However, this approach has some limitations. First, all the hydrated phases formed must be known and have a well-defined stoichiometry. This may occur in synthetic systems such as pure C_3S pastes, where the stoichiometry of portlandite and C-S-H is known [16,153]. For PC pastes (without SCMs), it seems reasonable to assume that only C_3S significantly contributes to C-S-H formation within the first one or two days of hydration [53,154]. However, accurately quantifying poorly crystalline hydrated phases such as AFm (see Section 4.5) may be difficult, possibly leading to errors in estimating the water consumed by these phases. When it comes to calcium (sulfo)aluminate systems, the formation of different amorphous/nanocrystalline hydrated phases may require the support of ^{1}H NMR for free water quantification [72,138].

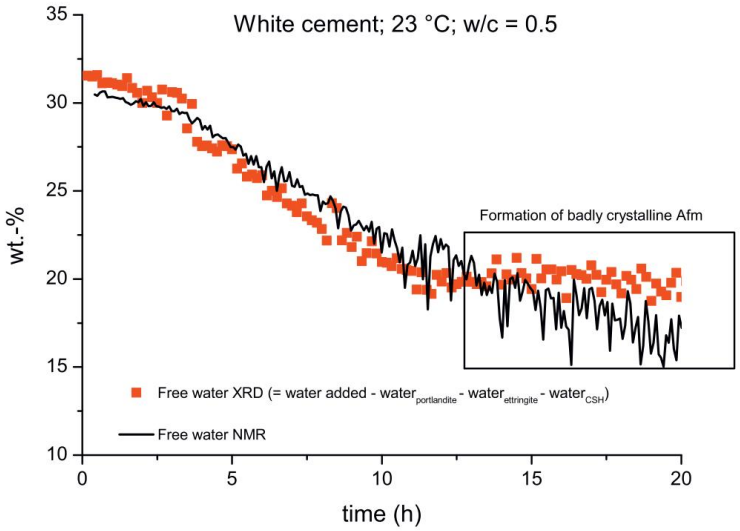

Figure 17. Comparison between free water from XRD and ^{1}H NMR during white Portland cement hydration (23 °C; w/s = 0.5). Reproduced from [46] with permission from Elsevier.

4.3. Water evaporation

Since the external standard method used for QPA is based on the sample MAC, which depends on the chemical composition of the sample (see Section 3.3), water evaporation changes the MAC of the sample over time and leads to erroneous QPA results. This fact is disregarded in most reports in the literature. However, Hüller et al. [155] and Goergens *et al.* [77] recently demonstrated that a significant water loss might occur during *in-situ* XRD tests (illustrated in Figure 18), which is more marked as the temperature increases. For instance, at 23 °C (the testing temperature usually adopted), a mixing water loss of 10 wt% (around 3 wt% of the sample) was observed after 32 hours. Considering that the MAC of PC usually ranges within 94-100 cm²/g for CuKα [103,114,126], a fresh PC paste with a w/c ratio of 0.5 would have a MAC of about 68 cm²/g. A 10% reduction in its water content would lead to a MAC of 70 cm²/g, resulting in a systematic relative error of 3% in QPA results. In general, this would fall within the error of the QPA for *in-situ* XRD, of around 2 wt% for major phases and 1 wt% for minor phases (see Section 4.2). However, this issue becomes important when considering the water loss at 40 °C (about 33 wt% of the mixing water or 10 wt% of the sample), which would lead to a systematic relative error of 11% in QPA results. Thus, some solutions can be adopted to improve the accuracy of QPA in situations where the sample faces significant water loss: (i) use an XRD system with controlled humidity [10,156]; or (ii) use a sample holder that reduces water loss, *e.g.*, glass capillaries sealed with wax.

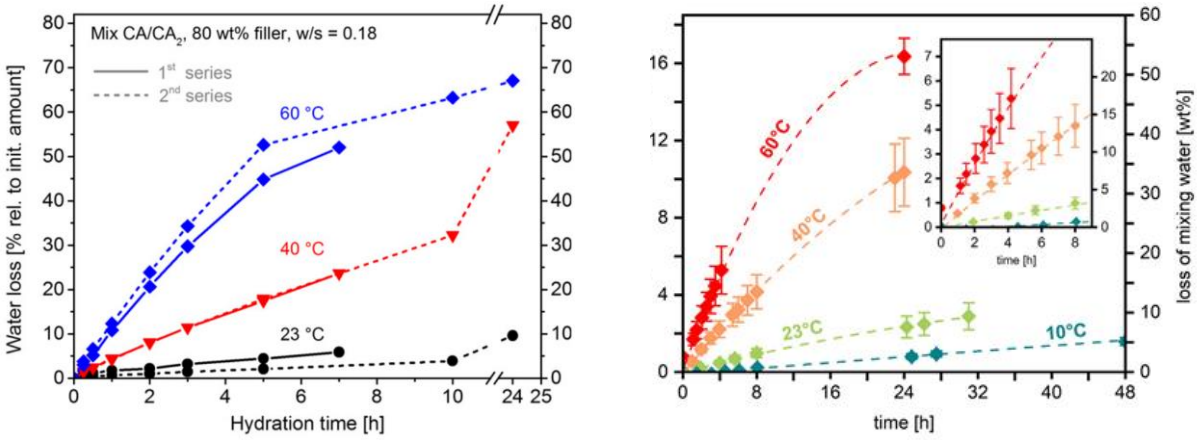

(a) (b)

Figure 18. Water loss over time for *in-situ* XRD measurements at different temperatures. (a) from [155], reproduced with permission from Wiley; (b) from [77], reproduced with permission from Elsevier.

4.4. Preferred orientation

Preferred orientation is an undesired alignment of crystals that impairs the random distribution required for proper XRD data collection. Sample spinning during data collection is mandatory to obtain accurate XRD data and minimize preferred orientation or the texture effects [157]. This issue can be faced in powder XRD due to sample preparation, especially for front pressed sample loading [13,145]. The use of fresh paste for *in-situ* XRD measurements avoids the particle orientation faced in powder XRD preparation. However, the use of a foil to cover the fresh sample can induce the preferred orientation on the paste/film interface, especially for elongated (*e.g.*, gypsum) and flat (*e.g.*, portlandite) crystals. Preferred orientation can be (partially) corrected in the refinement, for instance, by using the March-Dollase (M-D) [158] or spherical-harmonic (SH) functions [159]. In this regard, De la Torre *et al.* [160] demonstrated that SH correction (with order-8) led to more accurate QPA results than M-D correction in powder gypsum:corundum samples with 50:50 wt%. In turn, high order SH correction was required for lower gypsum contents but no further resolved peaks to optimize the parameters, so M-D correction was indicated.

In the case of fresh cement paste covered with Kapton, using the M-D function to correct the preferred orientation of gypsum may be tricky. The main reflections of this phase match with the range of the Kapton film signal (~10-30° 2θ for CuKα radiation), as illustrated in Figure 19a. In addition, gypsum is usually present in low contents in PC pastes: around 5 wt% of the solid fraction and 3 wt% of fresh paste. In these pastes, the only gypsum reflection that is not significantly overlapped by other anhydrous or hydrated phases is at around 11.6° 2θ (for CuKα radiation), as demonstrated in Figure 19b. This corresponds to the reflection from the (0 2 0) plane, which faces the highest preferred orientation issue. Thus, relying on this single peak as the input for M-D correction may be risky, but perhaps this is the best strategy since SH correction for a phase present in such low content is not recommended.

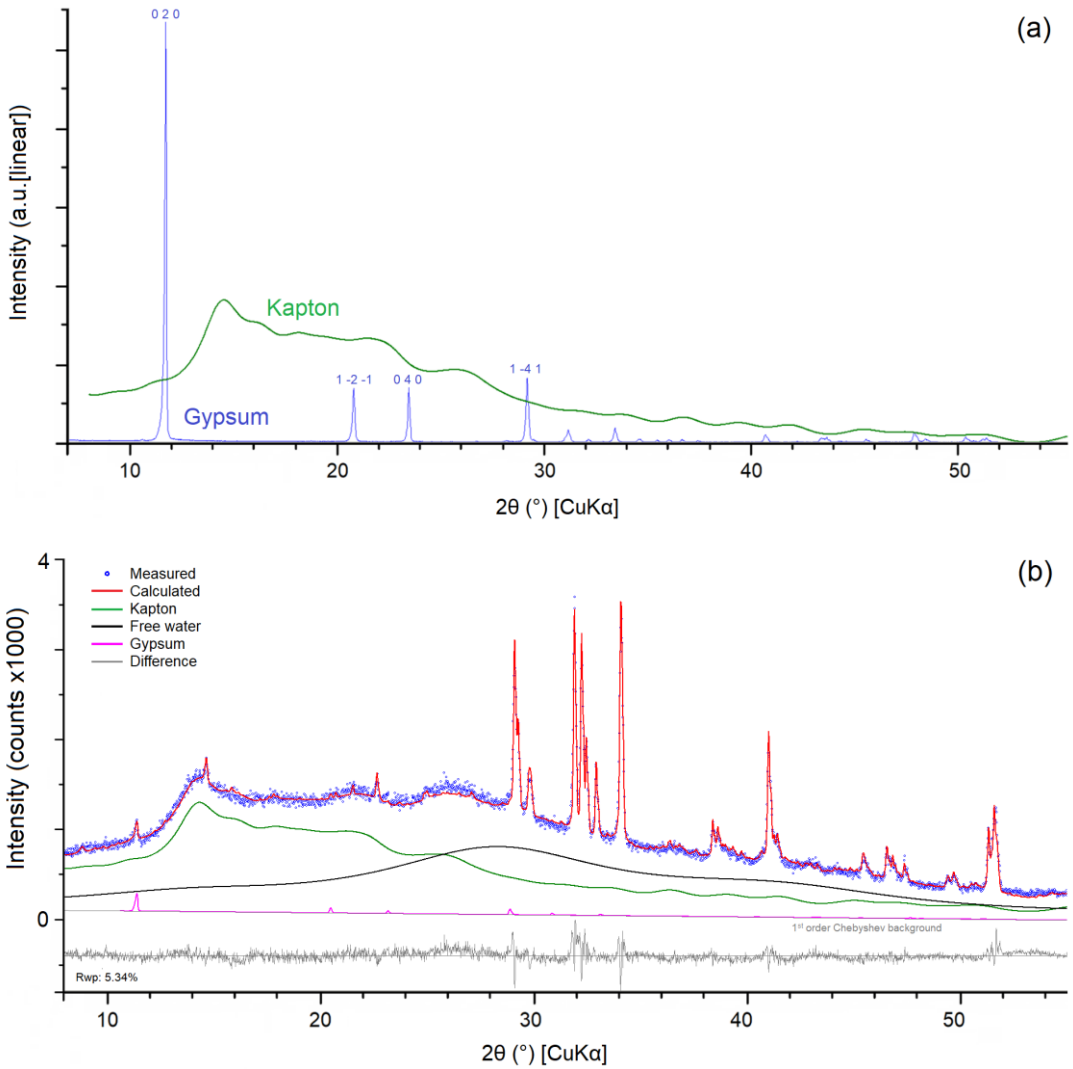

Figure 19. Gypsum identification in *in-situ* XRD experiments. (a) gypsum signal modeled in a pure powder sample, and Kapton modeled signal; (b) C_3S-C_3A-gypsum paste at 0.5 hours of hydration (23 °C; w/s = 0.5). Data from [37].

4.5. Amorphous or non-crystalline phases

The presence of amorphous or non-crystalline (ACn) phases can turn the XRD pattern fitting difficult due to the lack of a well-defined crystal structure. These phases can come from the cement hydration reactions or the anhydrous material; some authors recently reported ACn contents of up to 15-20 wt% in anhydrous non-blended Portland and CSA cements [73,149,154]. It is stressed that, for *in-situ* XRD, QPA is usually conducted using the external standard method, which yields the absolute weight fraction of each phase. So, the presence of ACn phases does not impair the quantification of the crystalline phases as long as the ACn's are properly fitted in the XRD pattern.

Besides calcium silicate and calcium aluminate hydrates (already discussed in Section 3.2), perhaps the most common poorly crystalline phases found in hydrated pastes are AFm's. According to Ectors [161], the layered nature of AFm-type structures often results in stacking disorder and

anisotropic peak broadening in XRD, making their crystal structure determination difficult and preventing its accurate quantification. Jansen *et al.* [46] observed lower hemicarbonate formation than expected from the C_3A dissolution in *in-situ* measurements of PC pastes, attributing it to the low crystallinity of the AFm phase. Cuesta *et al.* [98] also reported the difficulty of fitting the range of the main AFm peaks (around 8-12° 2θ for CuKα radiation) in synthetic ye'elimite samples, observing the presence of unknown AFm phases (most likely $C_4A\bar{S}H_{12}$). Ectors *et al.* [35] observed the presence of AFm phases with partially known crystal structures (*e.g.*, sulfate-AFm-16 and hydroxy-AFm-19) in *in-situ* XRD measurements of synthetic brownmillerite-calcium sulfate-calcite systems, preventing the accurate determination of the weight fraction of these phases. In high-alkalinity media, U-phase can be formed, which corresponds to a Na-substituted AFm phase [162,163]. Andrade Neto *et al.* [31] observed the formation of U-phase in C_3A-gypsum pastes when sodium was incorporated in either the mixing water (with NaOH addition) or the C_3A crystal structure (Na-doped orthorhombic C_3A).

Therefore, the quantitative analysis of non/poorly crystalline phases over time is often conducted through semi-quantitative approaches such as evaluating their relative scale factor, as discussed in Section 3.3 and seen in Figure 12. This reinforces the need for additional techniques to support the *in-situ* XRD results discussed next.

5. Technique association

Despite the good accuracy of *in-situ* XRD (detailed in Section 4.2), using additional techniques to support the data is highly recommended. The most common technique used for this purpose is the isothermal calorimetry due to its good reproducibility (assuming that the equipment is calibrated and the experimental procedures and analyses were adequately conducted), besides providing a continuous measurement without sample disturbance like *in-situ* XRD. Figure 20 shows an example of an *in-situ* XRD vs. calorimetry plot from Dittrich *et al.* [53]. A good agreement between the end of the induction period and the beginning of alite (C_3S) dissolution (marked as A) is observed. Similarly, the sulfate depletion point in calorimetry (marked as B) matched the anhydrite exhaustion and the renewed C_3A dissolution with quick ettringite formation. Furthermore, Jansen *et al.* [45] and Hesse et al. [38] compared the heat release expected from phase dissolution and precipitation calculated from *in-situ* XRD with that measured by calorimetry. The authors observed that the dissolutions of C_3S and C_3A, and the precipitation of C-S-H, portlandite, and ettringite were the main responsible for the heat released within the first 22 hours, while anhydrite and gypsum dissolutions had a marginal contribution to the heat release. Klaus et al. [164] used the same approach in order to prove the reactivity of CA_2 in a CAC system.

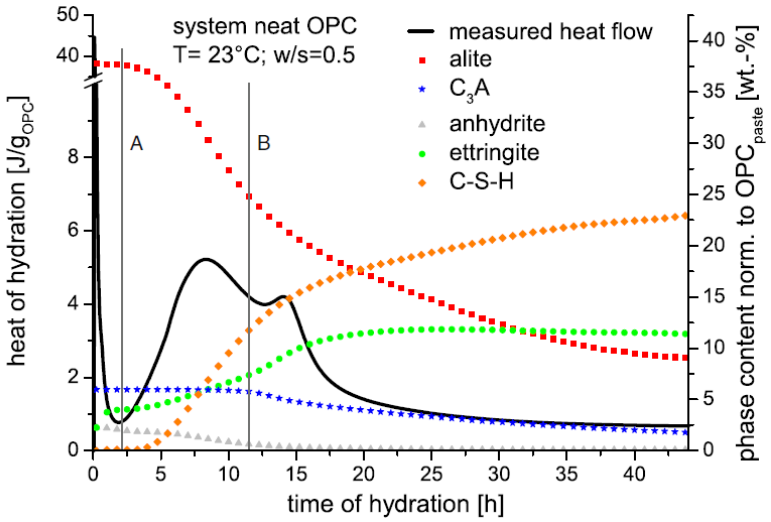

Figure 20. Example of technique association for PC paste: *in-situ* XRD and isothermal calorimetry (23 °C; w/s = 0.5). Reproduced from [53] with permission from Elsevier.

Powder XRD can also be used to support *in-situ* XRD results. Ma *et al.* [73] coupled *in-situ* XRD (up to 20 hours) and powder XRD (up to 28 days) to evaluate the effect of incorporating ye'elimite in C_3S clinker. Sun and Vollpracht [78] used powder XRD to confirm their *in-situ* XRD data when evaluating NaOH-activated fly ash, metakaolin, and slag mixes. Redondo-Soto *et al.* [57] compared *in-situ* and powder XRD with strictly monochromatic MoKα_1 radiation (besides TGA, discussed next) from samples with 67 wt% PC, 30 wt% metakaolin, and 3 wt% gypsum; the results are shown in Figure 21. One can see that *in-situ* XRD yielded similar results to well-established powder XRD, confirming the accuracy of the former. However, attention must be given to sampling disturbance due to sample preparation, as discussed in Section 4.1.

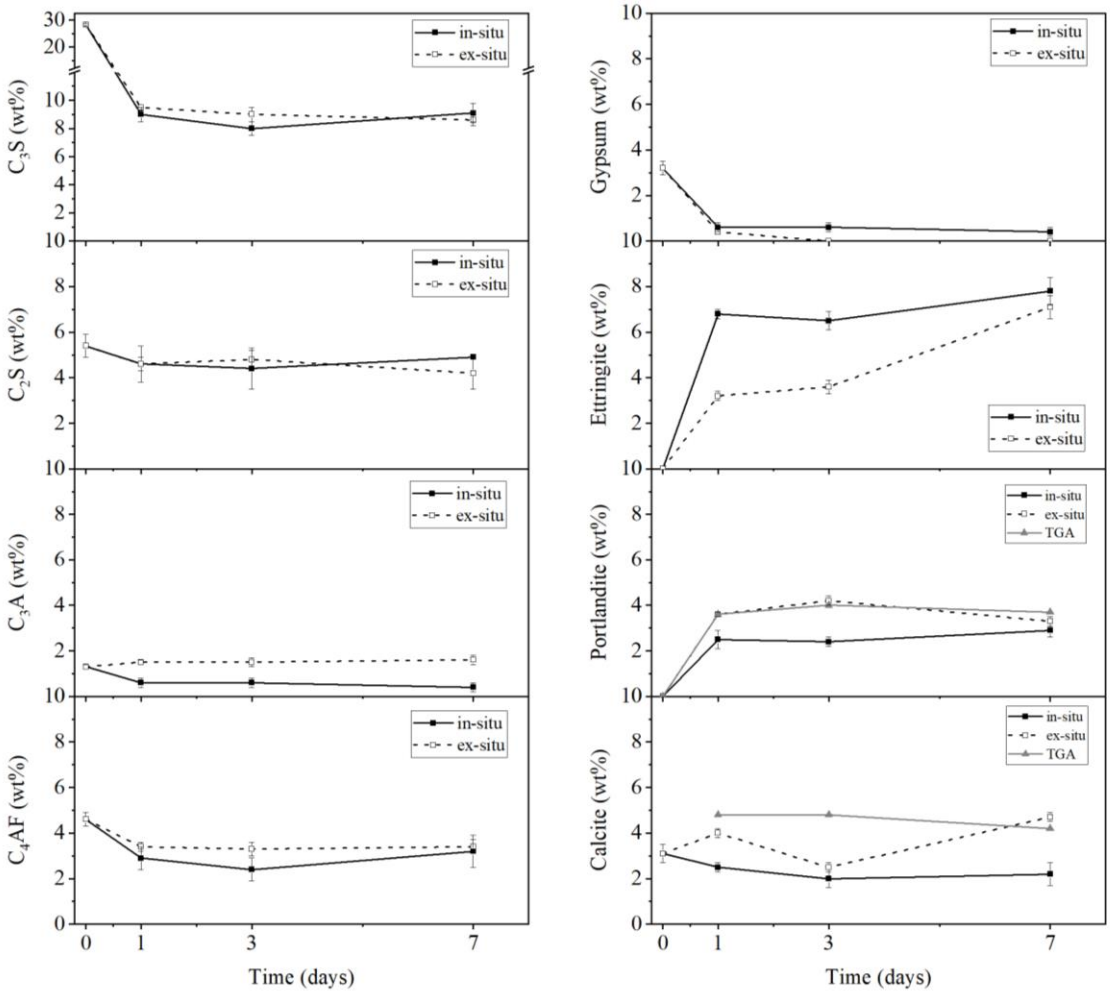

Figure 21. QPA results of *in-situ* and *ex-situ* MoKα_1 XRD, and TGA for a PC-MK-gypsum paste (w/s = 0.5). Error bars correspond to the estimated error. Data from [57].

Another valuable tool to support *in-situ* XRD is TGA. Jansen *et al.* [46] used TGA to confirm the formation of hemicarbonate after 13 hours of hydration in PC paste containing 2.8 wt% calcite. The authors observed divergences in the *in-situ* XRD QPA values for ettringite (consumed) and hemicarbonate (formed), associating it to the low crystallinity (and difficult quantification) of the AFm. Similarly, Andrade Neto *et al.* [31] observed the presence of $Al(OH)_3$ in C_3A-gypsum/bassanite pastes by TGA, which was not detected by *in-situ* XRD due to its low crystallinity as reported by [165]. Redondo-Soto *et al.* [57] compared results from TGA with *in-situ* and powder MoKα_1 XRD for the samples mentioned above. TGA was used to determine the amounts of portlandite and calcite following Ref. [166], shown in Figure 21. The results from TGA validated the *in-situ* analysis, although the relative errors in Rietveld QPA may be as high as 100% for minor phases (see Section 4.2).

In-situ XRD gives a reasonable description of the well crystalline phases dissolved and precipitated during cement hydration. However, the existence of amorphous phases complicates the interpretation of the results. In this case, other methods have to be used in order to get a complete picture of the reactions running. Several methods are thinkable to be combined with *in-situ* XRD. First

of all, NMR experiments [167] can give detailed insights into the state of several elements from interest during cement hydration and give information about phases dissolved and formed. This, in turn, is very often mandatory for answering specific questions concerning cement hydration. Due to the high equipment cost and measurement time, the method acquires much more effort. However, ^{1}H-TD-NMR [168] is becoming more important in cement hydration studies. It can give information on the state of the hydrogen in the sample and consequently can give detailed indications about hydrate phases formed. Due to the comparably low equipment costs and the availability of powerful PCs, the evaluation of real *in-situ* measurements applying ^{1}H-TD-NMR with a time resolution within the minute range can be evaluated [169]. This additional information can help identify different water contents of the hydrate phases formed and provide guidance about other amorphous phases formed.

An example is the existence of the phase CAH_{10} during hydration of CSA-type cements, which was proven to be formed but is not always from crystalline nature [170]. In this case, additional methods like thermodynamic modeling, scanning transmission electron microscopy images [171], or ^{1}H-TD-NMR [72] can give information about the phase formed and prove its existence. The same can be seen in ternary CSA-PC-anhydrite with the addition of Li_2CO_3, in which an amorphous Si-containing phase is formed but cannot be detected by *in-situ* XRD. In this case, NMR experiments are limited due to the high iron content, but pore solution analysis and the calculation of saturation indices can help to identify at least possible phases formed such as C_2ASH_8 or zeolite [74].

One of the major goals of cement hydration studies is certainly to predict reactions in terms of products but also in the case of kinetics, which means how a reaction will proceed. The prediction of thermodynamic stable hydrate phase assemblage has been used now for a long time [172–174]. However, concerning *in-situ* XRD, it is also of high interest why specific hydrate phases are formed and why the phases are also dissolved over hydration time, as seen in Figure 22. The key to understanding such reactions lies in the solubility of the phases formed in the system examined. As an example, the system Ca-Al-C will be discussed here. Figure 22a shows the solubility curves of the phases which can be formed in the system. In order to get an idea about the reaction kinetics, it is mandatory to know the initial pore solution and the thermodynamic equilibrium, as indicated in Figure 22a. Several phases such as monocarbonate (MC), hemicarbonate (HC), C_2AH_8 and AH are oversaturated at the start of the reaction. During hydration, the system evolves towards the thermodynamic equilibrium, which is in the system examined a phase assemblage of MC and AH. Consequently, the initial phases formed such as CAH_{10} and C_2AH_8 have to be dissolved again. *In-situ* XRD exactly proves the thermodynamic considerations (Figure 22b). After a certain induction period where the stable nucleation occurs, the initially oversaturated phases MC, AH, CAH_{10} and C_2AH_8 are formed. During the evolution of the system towards the thermodynamic equilibrium, the initially formed phases are subsequently dissolved again as soon as the solubility curve is crossed again towards undersaturation. Similar work without applying *in-situ* XRD can be found in the literature [172,173].

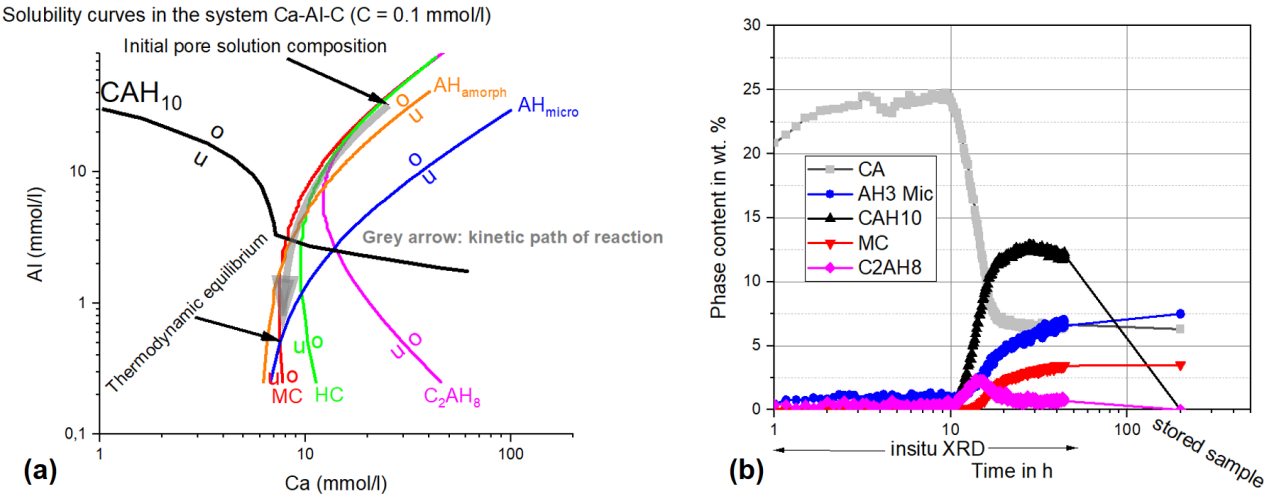

Figure 22. Solubility curves (a) and XRD QPA (b) of a Ca-Al-C system (C = 0.1 mmol/l). Data from [175].

Furthermore, *in-situ* XRD can help understand other important key parameters for cementitious materials such as rheology. Jakob et al. [49] coupled *in-situ* XRD and rheological measurements to correlate the ettringite formation with the rheological changes in PC pastes. The authors associated the increase in the measured torque within the first two hours of hydration with the increase in its solid fraction (due to the water consumption by ettringite formation), relating it with the well-known Krieger-Dougerthy model [176]. Pott *et al.* [65] used rheological tests and SEM coupled with *in-situ* XRD and isothermal calorimetry to investigate incompatibilities between PC and polycarboxylate-ether superplasticizer. The authors demonstrated that incorporating superplasticizer in a high dosage prevented the passivation of the aluminate phases of cement, inducing the quick formation of ettringite and hemicarbonate and resulting in severe workability loss. Andrade Neto *et al.* [31] used in-situ XRD, calorimetry, TGA, SEM, and rotational rheometry to explain the effect of incorporating either gypsum or hemihydrate in C_3A pastes. The authors observed that gypsum was detected up to 8-36 hours of hydration (depending on the C_3A polymorph), while hemihydrate was not detected from the first measurement (at 30 minutes of hydration) since it was quickly hydrated, precipitating large gypsum crystals (confirmed by SEM). This hydration consumed a significant amount of water, drastically impairing the workability of the pastes to the point that it was not possible to carry out rheological tests 10 minutes after mixing.

6. Summary and conclusion

In-situ laboratory XRD has proven to be a powerful tool for assessing the hydration of cementitious materials. It allows to qualitatively distinguish phases that are often overlapped in other techniques (*e.g.*, in TGA), in addition to providing a quantitative analysis with reasonable precision (in general, 1-2 wt%). Besides, the absence of hydration stoppage allows several measurements over time and avoids phase degradation. However, some care must be taken during testing and analyses.

Adopting a proper experimental setup is essential to collect data within a short period (around 10-15 minutes) while keeping adequate statistics; maximum intensity counts above the background of around 3000-5000 are desired. The sample holder should be chosen considering the sample fluidity and the risk of segregation. The simultaneous presence of different amorphous contributions in the XRD patterns (*e.g.*, Kapton foil, free water, C-(A)-S-H, SCMs) requires the creation and calibration of independent models. The use of an adequate data analysis routine improves the consistency of the time-resolved studies and reduces the variability between operators, besides avoiding unrealistic results. The global and phase parameters that must be considered in the data analysis were discussed.

One must be aware of the limitations of this technique, such as its precision and detection limit, sample preparation, preferred orientation, water evaporation, and segregation issues. Independent techniques are highly recommended to support the *in-situ* XRD data, *e.g.*, isothermal calorimetry, TGA, powder XRD, and NMR. Finally, a round robin test to assess the reproducibility of laboratory *in-situ* XRD measurements (as already reported for powder XRD) is suggested.

Declaration of competing interest

The authors declare that they have no known competing financial interests or personal relationships that could have influenced the work reported in this paper.

Acknowledgments

PRM, JSAN, CEMC, and APK acknowledge the financial support of the following Brazilian governmental agencies CAPES (Coordination for the Improvement of Higher Education Personnel), CNPq (Brazilian National Council for Scientific and Technological Development) and FAPERGS (Foundation for Research Support of the State of Rio Grande do Sul). AGDT acknowledges PID2020-114650RB-I00 grand from the Spanish government. XRD experiments were carried out at the LDRX-UFSC Multiuser facility. Rafael Sakata is kindly acknowledged for the assistance in XRD experiments; Irina Kirchberger is acknowledged for the AFm data used in Section 3.2.4; Cinthya Redondo-Soto is acknowledged for the Mo-XRD data and analysis. The two anonymous reviewers are gratefully acknowledged for their insightful contributions.

References

[1] K. Scrivener, A. Ouzia, P. Juilland, A. Kunhi Mohamed, Advances in understanding cement hydration mechanisms, Cem. Concr. Res. 124 (2019) 105823. https://doi.org/10.1016/j.cemconres.2019.105823.

[2] K.L. Scrivener, V.M. John, E.M. Gartner, Eco-efficient cements: Potential economically viable solutions for a low-CO2 cement-based materials industry, Cem. Concr. Res. 114 (2018) 2–26. https://doi.org/10.1016/j.cemconres.2018.03.015.

[3] M. Ben Haha, F. Winnefeld, A. Pisch, Advances in understanding ye'elimite-rich cements, Cem. Concr. Res. 123 (2019) 105778. https://doi.org/10.1016/j.cemconres.2019.105778.

[4] C. Shi, A.F. Jiménez, A. Palomo, New cements for the 21st century: The pursuit of an alternative to Portland cement, Cem. Concr. Res. 41 (2011) 750–763. https://doi.org/10.1016/j.cemconres.2011.03.016.

[5] E. Gartner, T. Sui, Alternative cement clinkers, Cem. Concr. Res. 114 (2018) 27–39. https://doi.org/10.1016/j.cemconres.2017.02.002.

[6] A. Cuesta, A. Ayuela, M.A.G. Aranda, Belite cements and their activation, Cem. Concr. Res. 140 (2021) 106319. https://doi.org/10.1016/j.cemconres.2020.106319.

[7] E. Gartner, What are BYF cements, and how do they differ from CSA cements?, Futur. Cem. 200 Years after Louis Vicat. (2017) 6–8. http://www.ecobinder-project.eu.

[8] C. Shi, B. Qu, J.L. Provis, Recent progress in low-carbon binders, Cem. Concr. Res. 122 (2019) 227–250. https://doi.org/10.1016/j.cemconres.2019.05.009.

[9] K. Scrivener, F. Martirena, S. Bishnoi, S. Maity, Calcined clay limestone cements (LC3), Cem. Concr. Res. 114 (2018) 49–56. https://doi.org/10.1016/j.cemconres.2017.08.017.

[10] K.L. Scrivener, T. Füllmann, E. Gallucci, G. Walenta, E. Bermejo, Quantitative study of Portland cement hydration by X-ray diffraction/Rietveld analysis and independent methods, Cem. Concr. Res. 34 (2004) 1541–1547. https://doi.org/10.1016/j.cemconres.2004.04.014.

[11] J.J. Wolf, D. Jansen, F. Goetz-Neunhoeffer, J. Neubauer, Application of thermodynamic modeling to predict the stable hydrate phase assemblages in ternary CSA-OPC-anhydrite systems and quantitative verification by QXRD, Cem. Concr. Res. 128 (2020). https://doi.org/10.1016/j.cemconres.2019.105956.

[12] J.S. Andrade Neto, E.D. Rodríguez, P.J.M. Monteiro, A.G. De la Torre, A.P. Kirchheim, Hydration of C3S and Al-doped C3S in the presence of gypsum, Cem. Concr. Res. 152 (2022) 106686. https://doi.org/10.1016/j.cemconres.2021.106686.

[13] G. Le Saoût, V. Kocaba, K. Scrivener, Application of the Rietveld method to the analysis of anhydrous cement, Cem. Concr. Res. 41 (2011) 133–148. https://doi.org/10.1016/j.cemconres.2010.10.003.

[14] H. Kazemi-Kamyab, A.C.A. Muller, E. Denarié, E. Brühwiler, K. Scrivener, Kinetics of mixing-water repartition in UHPFRC paste and its effect on hydration and microstructural development, Cem. Concr. Res. 124 (2019) 105784. https://doi.org/10.1016/j.cemconres.2019.105784.

[15] R. Snellings, G. Mertens, Ö. Cizer, J. Elsen, Early age hydration and pozzolanic reaction in natural zeolite blended cements: Reaction kinetics and products by in situ synchrotron X-ray powder, Cem. Concr. Res. 40 (2010) 1704–1713. https://doi.org/10.1016/j.cemconres.2010.08.012.

[16] A. Cuesta, J.D. Zea-Garcia, D. Londono-Zuluaga, A.G. De La Torre, I. Santacruz, O. Vallcorba, M. Dapiaggi, S.G. Sanfélix, M.A.G. Aranda, Multiscale understanding of tricalcium silicate hydration reactions, Sci. Rep. 8 (2018) 1–11. https://doi.org/10.1038/s41598-018-26943-y.

[17] G. Álvarez-Pinazo, A. Cuesta, M. García-Maté, I. Santacruz, E.R. Losilla, S.G. Sanfélix, F. Fauth, M.A.G. Aranda, A.G. De La Torre, In-situ early-age hydration study of sulfobelite cements by synchrotron powder diffraction, Cem. Concr. Res. 56 (2014) 12–19. https://doi.org/10.1016/j.cemconres.2013.10.009.

[18] L. Morejón-Alonso, M. Motisuke, J.R. Correa, R.G. Carrodeguas, L.A. Dos Santos, In situ synchrotron x-ray powder diffraction study of the early hydration of α-tricalcium phosphate/tricalcium silicate composite bone cement, Mater. Res. 18 (2015) 164–169. https://doi.org/10.1590/1516-1439.302114.

[19] J. Luo, F.J. Martinez-Casado, O. Balmes, J. Yang, C. Persson, H. Engqvist, W. Xia, In Situ Synchrotron X-ray Diffraction Analysis of the Setting Process of Brushite Cement: Reaction and Crystal Growth, ACS Appl. Mater. Interfaces. 9 (2017) 36392–36399. https://doi.org/10.1021/acsami.7b10159.

[20] M. Merlini, C. Meneghini, G. Artioli, T. Cerulli, Synchrotron radiation XRPD study on the early hydration of cements, Zeitschrift Fur Krist. Suppl. 2 (2007) 411–416. https://doi.org/10.1524/zksu.2007.2007.suppl_26.411.

[21] C.W. Hargis, A.P. Kirchheim, P.J.M. Monteiro, E.M. Gartner, Early age hydration of calcium sulfoaluminate (synthetic ye'elimite, $C_4A_3\bar{S}$) in the presence of gypsum and varying amounts of

calcium hydroxide, Cem. Concr. Res. 48 (2013) 105–115. https://doi.org/10.1016/j.cemconres.2013.03.001.

[22] L. Valentini, M.C. Dalconi, M. Favero, G. Artioli, G. Ferrari, In-Situ XRD measurement and quantitative analysis of hydrating cement: Implications for sulfate incorporation in C-S-H, J. Am. Ceram. Soc. 98 (2015) 1259–1264. https://doi.org/10.1111/jace.13401.

[23] B. Mota, T. Matschei, K. Scrivener, The influence of sodium salts and gypsum on alite hydration, Cem. Concr. Res. 75 (2015) 53–65. https://doi.org/10.1016/j.cemconres.2015.04.015.

[24] S.T. Bergold, F. Goetz-Neunhoeffer, J. Neubauer, Quantitative analysis of C-S-H in hydrating alite pastes by in-situ XRD, Cem. Concr. Res. 53 (2013) 119–126. https://doi.org/10.1016/j.cemconres.2013.06.001.

[25] H.M. Jennings, Model for the microstructure of calcium silicate hydrate in cement paste, Cem. Concr. Res. 30 (2000) 101–116. https://doi.org/10.1016/S0008-8846(99)00209-4.

[26] A.J. Allen, J.J. Thomas, H.M. Jennings, Composition and density of nanoscale calcium-silicate-hydrate in cement, Nat. Mater. 6 (2007) 311–316. https://doi.org/10.1038/nmat1871.

[27] H.M. Jennings, Refinements to colloid model of C-S-H in cement: CM-II, Cem. Concr. Res. 38 (2008) 275–289. https://doi.org/10.1016/j.cemconres.2007.10.006.

[28] J. Plank, M. Schönlein, V. Kanchanason, Study on the early crystallization of calcium silicate hydrate (C-S-H) in the presence of polycarboxylate superplasticizers, J. Organomet. Chem. 869 (2018) 227–232. https://doi.org/10.1016/j.jorganchem.2018.02.005.

[29] A. Quennoz, K.L. Scrivener, Hydration of C 3A-gypsum systems, Cem. Concr. Res. 42 (2012) 1032–1041. https://doi.org/10.1016/j.cemconres.2012.04.005.

[30] A.P. Kirchheim, E.D. Rodríguez, R.J. Myers, L.A. Gobbo, P.J.M. Monteiro, D.C.C. Dal Molin, R.B. de Souza, M.A. Cincotto, Effect of gypsum on the early hydration of cubic and Na-doped orthorhombic tricalcium aluminate, Materials (Basel). 11 (2018) 1–16. https://doi.org/10.3390/ma11040568.

[31] J.S. Andrade Neto, P.R. de Matos, A.G. De la Torre, C.E.M. Campos, P.J.P. Gleize, P.J.M. Monteiro, A.P. Kirchheim, The role of sodium and sulfate sources on the rheology and hydration of C_3A polymorphs, Cem. Concr. Res. 151 (2022) 106639. https://doi.org/10.1016/j.cemconres.2021.106639.

[32] S. Wistuba, D. Stephan, G. Raudaschl-Sieber, J. Plank, Hydration and hydration products of two-phase Portland cement clinker doped with Na_2O, Adv. Cem. Res. 19 (2007) 125–131. https://doi.org/10.1680/adcr.2007.19.3.125.

[33] Y. Cai, D. Xuan, P. Hou, J. Shi, C.S. Poon, Effect of seawater as mixing water on the hydration behaviour of tricalcium aluminate, Cem. Concr. Res. 149 (2021) 106565. https://doi.org/10.1016/j.cemconres.2021.106565.

[34] R.J. Myers, G. Geng, J. Li, E.D. Rodríguez, J. Ha, P. Kidkhunthod, G. Sposito, L.N. Lammers, A.P. Kirchheim, P.J.M. Monteiro, Role of adsorption phenomena in cubic tricalcium aluminate dissolution, Langmuir. 33 (2016) 45–55. https://doi.org/10.1021/acs.langmuir.6b03474.

[35] D. Ectors, J. Neubauer, F. Goetz-Neunhoeffer, The hydration of synthetic brownmillerite in presence of low Ca-sulfate content and calcite monitored by quantitative in-situ-XRD and heat flow calorimetry, Cem. Concr. Res. 54 (2013) 61–68. https://doi.org/10.1016/j.cemconres.2013.08.011.

[36] M.T.T. Souza, P.R. de Matos, J.S. Andrade Neto, R.D. Sakata, C.E.M. de Campos, A.P.N. de Oliveira, O.R.K. Montedo, S. Arcaro, Single-burn clinkering of endodontic calcium silicate-based cements: Effects of ZnO in the C_3S phase formation and hydration rate, Mater. Lett. In press (2021).

[37] J.S. Andrade Neto, P.R. de Matos, A.G. de la Torre, C.E.M. Campos, S.M. Torres, P.J.M. Monteiro, A.P. Kirchheim, Hydration and interactions between pure and doped C_3S and C_3A in the presence of different calcium sulfates, Cem. Concr. Res. 159 (2022) 106893. https://doi.org/10.1016/j.cemconres.2022.106893.

[38] C. Hesse, F. Goetz-Neunhoeffer, J. Neubauer, A new approach in quantitative in-situ XRD of cement pastes: Correlation of heat flow curves with early hydration reactions, Cem. Concr. Res. 41 (2011) 123–128. https://doi.org/10.1016/j.cemconres.2010.09.014.

[39] C. Hesse, F. Goetz-Neunhoeffer, J. Neubauer, M. Braeu, P. Gaeberlein, Quantitative in situ X-ray diffraction analysis of early hydration of Portland cement at defined temperatures, Powder Diffr. 24 (2009) 112–115. https://doi.org/10.1154/1.3120603.

[40] A. Quennoz, K.L. Scrivener, Interactions between alite and C_3A-gypsum hydrations in model cements, Cem. Concr. Res. 44 (2013) 46–54. https://doi.org/10.1016/j.cemconres.2012.10.018.

[41] F. Zunino, K. Scrivener, Factors influencing the sulfate balance in pure phase C3S/C3A systems, Cem. Concr. Res. 133 (2020) 106085. https://doi.org/10.1016/j.cemconres.2020.106085.

[42] H. Pöllmann, R. Wenda, M. Fylak, Combination of cryo-SEM, in-situ XRD and heat-flow calorimetry for early time hydration studies of Portland cements, in: Proc. 30th Int. Conf. Cem. Microsc., 2008.

[43] H. Pöllmann, Application of Cryo-SEM microscopy and in-situ X-ray diffraction for the investigation of building material hydration, J. Wuhan Univ. Technol. 33 (2011) 1–10.

[44] D. Jansen, F. Goetz-Neunhoeffer, C. Stabler, J. Neubauer, A remastered external standard method applied to the quantification of early OPC hydration, Cem. Concr. Res. 41 (2011) 602–608. https://doi.org/10.1016/j.cemconres.2011.03.004.

[45] D. Jansen, F. Goetz-Neunhoeffer, B. Lothenbach, J. Neubauer, The early hydration of Ordinary Portland Cement (OPC): An approach comparing measured heat flow with calculated heat flow from QXRD, Cem. Concr. Res. 42 (2012) 134–138. https://doi.org/10.1016/j.cemconres.2011.09.001.

[46] D. Jansen, C. Naber, D. Ectors, Z. Lu, X.M. Kong, F. Goetz-Neunhoeffer, J. Neubauer, The early hydration of OPC investigated by in-situ XRD, heat flow calorimetry, pore water analysis and 1H NMR: Learning about adsorbed ions from a complete mass balance approach, Cem. Concr. Res. 109 (2018) 230–242. https://doi.org/10.1016/j.cemconres.2018.04.017.

[47] E.M.J. Bérodier, A.C.A. Muller, K.L. Scrivener, Effect of sulfate on C-S-H at early age, Cem. Concr. Res. 138 (2020). https://doi.org/10.1016/j.cemconres.2020.106248.

[48] E. Dubina, L. Black, R. Sieber, J. Plank, Interaction of water vapour with anhydrous cement minerals, Adv. Appl. Ceram. 109 (2010) 260–268. https://doi.org/10.1179/174367509X12554402491029.

[49] C. Jakob, D. Jansen, N. Ukrainczyk, E. Koenders, U. Pott, D. Stephan, J. Neubauer, Relating ettringite formation and rheological changes during the initial cement hydration: A comparative study applying XRD analysis, rheological measurements and modeling, Materials (Basel). 12 (2019). https://doi.org/10.3390/ma12182957.

[50] J. Schreiner, D. Jansen, D. Ectors, F. Goetz-Neunhoeffer, J. Neubauer, S. Volkmann, New analytical possibilities for monitoring the phase development during the production of autoclaved aerated concrete, Cem. Concr. Res. 107 (2018) 247–252. https://doi.org/10.1016/j.cemconres.2018.02.028.

[51] D. Ectors, F. Goetz-Neunhoeffer, J. Neubauer, A generalized geometric approach to anisotropic peak broadening due to domain morphology, J. Appl. Crystallogr. 48 (2015) 189–194. https://doi.org/10.1107/S1600576714026557.

[52] D. Ectors, F. Goetz-Neunhoeffer, J. Neubauer, Routine (an)isotropic crystallite size analysis in the double-Voigt approximation done right?, Powder Diffr. 32 (2017) S27–S34. https://doi.org/10.1017/S0885715617000070.

[53] S. Dittrich, J. Neubauer, F. Goetz-Neunhoeffer, The influence of fly ash on the hydration of OPC within the first 44 h - A quantitative in situ XRD and heat flow calorimetry study, Cem. Concr. Res. 56 (2014) 129–138. https://doi.org/10.1016/j.cemconres.2013.11.013.

[54] P.R. de Matos, R.D. Sakata, L. Onghero, V.G. Uliano, J. de Brito, C.E.M. Campos, P.J.P. Gleize, Utilization of ceramic tile demolition waste as supplementary cementitious material: An early-age investigation, J. Build. Eng. 38 (2021) 102187. https://doi.org/10.1016/j.jobe.2021.102187.

[55] G. Land, D. Stephan, The influence of nano-silica on the hydration of ordinary Portland cement, J. Mater. Sci. 47 (2012) 1011–1017. https://doi.org/10.1007/s10853-011-5881-1.

[56] F. Zunino, K. Scrivener, The influence of the filler effect on the sulfate requirement of blended cements, Cem. Concr. Res. 126 (2019) 105918. https://doi.org/10.1016/j.cemconres.2019.105918.

[57] C. Redondo-Soto, Angeles G. De la Torre, et al., Monitoring reaction degree of metakaolin by combined laboratory X-ray microtomography and powder diffraction, In Prep. (2022).

[58] M. García-Maté, A.G. De La Torre, L. León-Reina, E.R. Losilla, M.A.G. Aranda, I. Santacruz, Effect of calcium sulfate source on the hydration of calcium sulfoaluminate eco-cement, Cem. Concr. Compos. 55 (2015) 53–61. https://doi.org/10.1016/j.cemconcomp.2014.08.003.

[59] I.R. Salcedo, A. Cuesta, S. Shirani, L. León-Reina, M.A.G. Aranda, Accuracy in cement hydration investigations: Combined x-ray microtomography and powder diffraction analyses, Materials (Basel). 14 (2021). https://doi.org/10.3390/ma14226953.

[60] D. Jansen, J. Neubauer, F. Goetz-Neunhoeffer, R. Haerzschel, W.D. Hergeth, Change in reaction kinetics of a Portland cement caused by a superplasticizer - Calculation of heat flow curves from XRD data, Cem. Concr. Res. 42 (2012) 327–332. https://doi.org/10.1016/j.cemconres.2011.10.005.

[61] M.Y.A. Mollah, W.J. Adams, R. Schennach, D.L. Cocke, Review of cement-superplasticizer interactions and their models, Adv. Cem. Res. 12 (2000) 153–161. https://doi.org/10.1680/adcr.2000.12.4.153.

[62] P. Aïtcin, R.J. Flatt, Science and Technology of Concrete Admixtures, Woodhead Publishing Limited, 2016. https://doi.org/10.1016/C2015-0-00150-2.

[63] L. Valentini, M. Favero, M.C. Dalconi, V. Russo, G. Ferrari, G. Artioli, Kinetic Model of Calcium-Silicate Hydrate Nucleation and Growth in the Presence of PCE Superplasticizers, Cryst. Growth Des. 16 (2016) 646–654. https://doi.org/10.1021/acs.cgd.5b01127.

[64] P.R. de Matos, J.S. Andrade Neto, R.D. Sakata, C.E.M. Campos, A.P. Kirchheim, E.D. Rodríguez, Effect of superplasticizer addition time and metakaolin source on the early-age hydration of limestone calcined clay cement (LC3), Under Revi (2022).

[65] U. Pott, C. Jakob, D. Jansen, J. Neubauer, D. Stephan, Investigation of the incompatibilities of cement and superplasticizers and their influence on the rheological behavior, Materials (Basel). 13 (2020). https://doi.org/10.3390/ma13040977.

[66] V. Kanchanason, J. Plank, Effect of calcium silicate hydrate – polycarboxylate ether (C-S-H–PCE) nanocomposite as accelerating admixture on early strength enhancement of slag and calcined clay blended cements, Cem. Concr. Res. 119 (2019) 44–50. https://doi.org/10.1016/j.cemconres.2019.01.007.

[67] D. Jansen, Z. Lu, X.M. Kong, J. Pakusch, E. Jahns, F. Deschner, C. Schmidtke, The influence of the glass transition temperature (T g) of polymers on early OPC hydration: a complete study of the heat flow, phase evolution, and pore solution chemistry, Mater. Struct. Constr. 52 (2019). https://doi.org/10.1617/s11527-019-1435-9.

[68] X. Kong, J. Pakusch, D. Jansen, S. Emmerling, J. Neubauer, F. Goetz-Neuhoeffer, Effect of polymer latexes with cleaned serum on the phase development of hydrating cement pastes, Cem. Concr. Res. 84 (2016) 30–40. https://doi.org/10.1016/j.cemconres.2016.02.013.

[69] Z. Lu, X. Kong, D. Jansen, C. Zhang, J. Wang, X. Pang, J. Yin, Towards a further understanding of cement hydration in the presence of triethanolamine, Cem. Concr. Res. 132 (2020) 106041. https://doi.org/10.1016/j.cemconres.2020.106041.

[70] Z. Lu, X. Kong, D. Jansen, C. Zhang, A comparative study of the effects of two alkanolamines on cement hydration, Adv. Cem. Res. (2021) 1–10. https://doi.org/10.1680/jadcr.20.00063.

[71] T. Hirsch, Z. Lu, D. Stephan, Effect of different sulphate carriers on Portland cement hydration in the presence of triethanolamine, Constr. Build. Mater. 294 (2021) 123528. https://doi.org/10.1016/j.conbuildmat.2021.123528.

[72] D. Jansen, J.J. Wolf, N. Fobbe, The hydration of nearly pure ye'elimite with a sulfate carrier in a stoichiometric ettringite binder system. Implications for the hydration process based on in-situ XRD, 1H-TD-NMR, pore solution analysis, and thermodynamic modeling, Cem. Concr. Res. 127 (2020) 105923. https://doi.org/10.1016/j.cemconres.2019.105923.

[73] S. Ma, R. Snellings, X. Li, X. Shen, K.L. Scrivener, Alite-ye'elimite clinker: Hydration kinetics, products and microstructure, Constr. Build. Mater. 266 (2021) 121062. https://doi.org/10.1016/j.conbuildmat.2020.121062.

[74] J.J. Wolf, D. Jansen, F. Goetz-Neunhoeffer, J. Neubauer, Impact of varying Li_2CO_3 additions on the hydration of ternary CSA-OPC-anhydrite mixes, Cem. Concr. Res. 131 (2020) 106015. https://doi.org/10.1016/j.cemconres.2020.106015.

[75] A. Engbert, J. Plank, Templating effect of alginate and related biopolymers as hydration accelerators for calcium alumina cement - A mechanistic study, Mater. Des. 195 (2020) 109054. https://doi.org/10.1016/j.matdes.2020.109054.

[76] I. Galan, B. Müller, L.G. Briendl, F. Mittermayr, T. Mayr, M. Dietzel, C. Grengg, Continuous optical in-situ pH monitoring during early hydration of cementitious materials, Cem. Concr. Res. 150 (2021) 106584. https://doi.org/10.1016/j.cemconres.2021.106584.

[77] J. Goergens, T. Manninger, F. Goetz-Neunhoeffer, In-situ XRD study of the temperature-dependent early hydration of calcium aluminate cement in a mix with calcite, Cem. Concr. Res. 136 (2020). https://doi.org/10.1016/j.cemconres.2020.106160.

[78] Z. Sun, A. Vollpracht, Isothermal calorimetry and in-situ XRD study of the NaOH activated fly ash, metakaolin and slag, Cem. Concr. Res. 103 (2018) 110–122. https://doi.org/10.1016/j.cemconres.2017.10.004.

[79] R. Firdous, T. Hirsch, D. Klimm, B. Lothenbach, D. Stephan, Reaction of calcium carbonate minerals in sodium silicate solution and its role in alkali-activated systems, Miner. Eng. 165 (2021) 106849. https://doi.org/10.1016/j.mineng.2021.106849.

[80] K. Gijbels, H. Nguyen, P. Kinnunen, W. Schroeyers, Y. Pontikes, S. Schreurs, M. Illikainen, Feasibility of incorporating phosphogypsum in ettringite-based binder from ladle slag, J. Clean. Prod. 237 (2019) 117793. https://doi.org/10.1016/j.jclepro.2019.117793.

[81] Z. Zuhua, Y. Xiao, Z. Huajun, C. Yue, Role of water in the synthesis of calcined kaolin-based geopolymer, Appl. Clay Sci. 43 (2009) 218–223. https://doi.org/10.1016/j.clay.2008.09.003.

[82] M.M. Alonso, S. Gismera, M.T. Blanco, M. Lanzón, F. Puertas, Alkali-activated mortars: Workability and rheological behaviour, Constr. Build. Mater. 145 (2017) 576–587. https://doi.org/10.1016/j.conbuildmat.2017.04.020.

[83] L. Vitola, I. Pundiene, J. Pranckeviciene, D. Bajare, The impact of the amount of water used in activation solution and the initial temperature of paste on the rheological behaviour and structural evolution of metakaolin-based geopolymer pastes, Sustain. 12 (2020). https://doi.org/10.3390/su12198216.

[84] M.C. Dalconi, M. Favero, G. Artioli, In-situ XRPD of hydrating cement with lab instrument: reflection vs. transmission measurements, in: Eur. Powder Diffr. Conf. August 2010, Darmstadt, Ger., OLDENBOURG WISSENSCHAFTSVERLAG, 2011: pp. 155–162. https://doi.org/10.1524/9783486991321-028.

[85] M. Balonis, B. Lothenbach, G. Le Saout, F.P. Glasser, Impact of chloride on the mineralogy of hydrated Portland cement systems, Cem. Concr. Res. 40 (2010) 1009–1022. https://doi.org/10.1016/j.cemconres.2010.03.002.

[86] L.A. Gobbo, Application of X-ray diffraction and Rietveld method in the study of Portland cement (in Portuguese), Apl. Da Difração Raios X e Método Rietveld No Estud. Do Cim. Portl. (2009) 273. https://doi.org/https://teses.usp.br/teses/disponiveis/44/44137/tde-23072009-144653/pt-br.php.

[87] S.B. Feldman, P. Sandberg, D. Brown, F. Serafin, Phase Composition and Reaction Kinetics of OPC Hydration by In Situ Transmission XRD using a Focusing Elliptical Mirror, in: 12th Int. Congr. Chem. Cem., 2007.

[88] H. Wallander, J. Wallentin, Simulated sample heating from a nanofocused X-ray beam, J. Synchrotron Radiat. 24 (2017) 925–933. https://doi.org/10.1107/S1600577517008712.

[89] V. Honkimäki, J. Sleight, P. Suortti, Characteristic X-ray flux from sealed Cr, Cu, Mo, Ag and W tubes, J. Appl. Crystallogr. 23 (1990) 412–417. https://doi.org/10.1107/s0021889890006082.

[90] F. Deschner, B. Lothenbach, F. Winnefeld, J. Neubauer, Effect of temperature on the hydration of Portland cement blended with siliceous fly ash, Cem. Concr. Res. 52 (2013) 169–181. https://doi.org/10.1016/j.cemconres.2013.07.006.

[91] K. De Weerdt, M. Ben Haha, G. Le Saout, K.O. Kjellsen, H. Justnes, B. Lothenbach, The effect of temperature on the hydration of composite cements containing limestone powder and fly ash, Mater. Struct. Constr. 45 (2012) 1101–1114. https://doi.org/10.1617/s11527-011-9819-5.

[92] T.T.H. Bach, C.C.D. Coumes, I. Pochard, C. Mercier, B. Revel, A. Nonat, Influence of temperature on the hydration products of low pH cements, Cem. Concr. Res. 42 (2012) 805–817. https://doi.org/10.1016/j.cemconres.2012.03.009.

[93] B. Raab, H. Pöllmann, "C_2AH_8" – $2CaO{\cdot}Al_2O_3{\cdot}(8\pm n)H_2O$ – main hydration products of CAC, in: Eur. Powder Diffr. Conf. August 2010, Darmstadt, Ger., Oldenbourg Wissenschaftsverlag, 2011: pp. 349–354. https://doi.org/10.1524/9783486991321-058.

[94] A. Cuesta, G. Álvarez-Pinazo, M. García-Maté, I. Santacruz, M.A.G. Aranda, Á.G. De La Torre, L. León-Reina, Rietveld quantitative phase analysis with molybdenum radiation, Powder Diffr. 30 (2015) 25–35. https://doi.org/10.1017/S0885715614000785.

[95] M. García-Maté, G. Álvarez-Pinazo, L. León-Reina, A.G. De la Torre, M.A.G. Aranda, Rietveld quantitative phase analyses of SRM 2686a: A standard Portland clinker, Cem. Concr. Res. 115 (2019) 361–366. https://doi.org/10.1016/j.cemconres.2018.09.011.

[96] P. Riello, P. Canton, G. Fagherazzi, Calibration of the monochromator bandpass function for the X-ray Rietveld analysis, Powder Diffr. 12 (1997) 160–166. https://doi.org/10.1017/S0885715600009647.

[97] M. García-Maté, G. Álvarez-Pinazo, L. León-Reina, A.G. De la Torre, M.A.G. Aranda, Rietveld quantitative phase analyses of SRM 2686a: A standard Portland clinker, Cem. Concr. Res. 115 (2019) 361–366. https://doi.org/10.1016/j.cemconres.2018.09.011.

[98] A. Cuesta, G. Álvarez-Pinazo, S.G. Sanfélix, I. Peral, M.A.G. Aranda, A.G. De La Torre, Hydration mechanisms of two polymorphs of synthetic ye'elimite, Cem. Concr. Res. 63 (2014) 127–136. https://doi.org/10.1016/j.cemconres.2014.05.010.

[99] R.W. Cheary, A.A. Coelho, Axial Divergence in a Conventional X-ray Powder Diffractometer. I. Theoretical Foundations, J. Appl. Crystallogr. 31 (1998) 851–861. https://doi.org/10.1107/S0021889898006876.

[100] M.R. Rowles, The effect of data quality and model parameters on the quantitative phase analysis of X-ray diffraction data by the Rietveld method, J. Appl. Crystallogr. 54 (2021) 878–894. https://doi.org/10.1107/s160057672100371x.

[101] D. Jansen, S.T. Bergold, F. Goetz-Neunhoeffer, J. Neubauer, The hydration of alite: A time-resolved quantitative X-ray diffraction approach using the G-factor method compared with heat release, J. Appl. Crystallogr. 44 (2011) 895–901. https://doi.org/10.1107/S0021889811025933.

[102] Y.P. Stetsko, N. Shanahan, H. Deford, A. Zayed, Quantification of supplementary cementitious content in blended Portland cement using an iterative Rietveld-PONKCS technique, J. Appl. Crystallogr. 50 (2017) 498–507. https://doi.org/10.1107/S1600576717002965.

[103] R. Snellings, A. Salze, K.L. Scrivener, Use of X-ray diffraction to quantify amorphous supplementary cementitious materials in anhydrous and hydrated blended cements, Cem. Concr. Res. 64 (2014) 89–98. https://doi.org/10.1016/j.cemconres.2014.06.011.

[104] S.T. Bergold, F. Goetz-Neunhoeffer, J. Neubauer, Mechanically activated alite: New insights into alite hydration, Cem. Concr. Res. 76 (2015) 202–211. https://doi.org/10.1016/j.cemconres.2015.06.005.

[105] S.T. Bergold, D. Jansen, S. Dittrich, F. Goetz-Neunhoeffer, J. Neubauer, Development of C-S-H during the early hydration of alite with water at different temperatures: direct quantification by in-situ XRD, (2012) 91–96.

[106] M. Maier, R. Sposito, N. Beuntner, K.C. Thienel, Particle characteristics of calcined clays and limestone and their impact on early hydration and sulfate demand of blended cement, Cem. Concr. Res. 154 (2022) 106736. https://doi.org/10.1016/j.cemconres.2022.106736.

[107] S. Scherb, M. Maier, N. Beuntner, K.C. Thienel, J. Neubauer, Reaction kinetics during early hydration of calcined phyllosilicates in clinker-free model systems, Cem. Concr. Res. 143 (2021) 106382. https://doi.org/10.1016/j.cemconres.2021.106382.

[108] R. Snellings, X-ray powder diffraction applied to cement, in: K. Scrivener, R. Snellings, B. Lothenbach (Eds.), A Pract. Guid. to Microstruct. Anal. Cem. Mater., 1st ed., CRC Press, 2016: pp. 107–176.

[109] X. Li, R. Snellings, K.L. Scrivener, Quantification of amorphous siliceous fly ash in hydrated blended cement pastes by X-ray powder diffraction, J. Appl. Crystallogr. 52 (2019) 1358–1370. https://doi.org/10.1107/S1600576719013955.

[110] S. Scherb, N. Beuntner, K.C. Thienel, J. Neubauer, Quantitative X-ray diffraction of free, not chemically bound water with the PONKCS method, J. Appl. Crystallogr. 51 (2018) 1535–1543. https://doi.org/10.1107/S1600576718012888.

[111] M. Maier, S. Scherb, A. Neißer-Deiters, N. Beuntner, K.C. Thienel, Hydration of cubic tricalcium aluminate in the presence of calcined clays, J. Am. Ceram. Soc. 104 (2021) 3619–3631. https://doi.org/10.1111/jace.17745.

[112] E. Bonaccorsi, S. Merlino, A.R. Kampf, The crystal structure of tobermorite 14 Å (plombierite), a C-S-H phase, J. Am. Ceram. Soc. 88 (2005) 505–512. https://doi.org/10.1111/j.1551-2916.2005.00116.x.

[113] P.T. Durdziński, M. Ben Haha, M. Zajac, K.L. Scrivener, Phase assemblage of composite cements, Cem. Concr. Res. 99 (2017) 172–182. https://doi.org/10.1016/j.cemconres.2017.05.009.

[114] M. Mejdi, W. Wilson, M. Saillio, T. Chaussadent, L. Divet, A. Tagnit-Hamou, Quantifying glass powder reaction in blended-cement pastes with the Rietveld-PONKCS method, Cem. Concr. Res. 130 (2020) 105999. https://doi.org/10.1016/j.cemconres.2020.105999.

[115] G. Renaudin, J. Russias, F. Leroux, F. Frizon, C. Cau-dit-Coumes, Structural characterization of C-S-H and C-A-S-H samples-Part I: Long-range order investigated by Rietveld analyses, J. Solid State Chem. 182 (2009) 3312–3319. https://doi.org/10.1016/j.jssc.2009.09.026.

[116] A. Cuesta, I. Santacruz, A.G. De la Torre, M. Dapiaggi, J.D. Zea-Garcia, M.A.G. Aranda, Local structure and Ca/Si ratio in C-S-H gels from hydration of blends of tricalcium silicate and silica fume, Cem. Concr. Res. 143 (2021) 106405. https://doi.org/10.1016/j.cemconres.2021.106405.

[117] N.V.Y. Scarlett, I.C. Madsen, Quantification of phases with partial or no known crystal structures, Powder Diffr. 21 (2006) 278–284. https://doi.org/10.1154/1.2362855.

[118] J. Goergens, A. Koehler, F. Goetz-Neunhoeffer, Calibration and quantitative analysis of C_2AHx ($2CaO{\cdot}Al_2O3{\cdot}xH_2O$) by Rietveld refinement combined G-factor method, Cem. Concr. Res. 158 (2022) 106854. https://doi.org/10.1016/j.cemconres.2022.106854.

[119] R. Allmann, Refinement of the hybrid layer structure $[Ca_2Al(OH)_6]$ + • [1/2 SO_4 • $3H_2O$], Neues Jahrb. Für Mineral. 3 (1977) 136–144.

[120] J. Nehring, J. Neubauer, S. Berger, F. Goetz-Neunhoeffer, Acceleration of OPC by CAC in binary and ternary systems: The role of pore solution chemistry, Cem. Concr. Res. 107 (2018) 264–274. https://doi.org/10.1016/j.cemconres.2018.02.012.

[121] H. Pöllmann, AFm-phase in cementitious materials, in: Proceeding 33rd Int. Conf. Cem. Microsc., 2011.

[122] L.G. Baquerizo, T. Matschei, K.L. Scrivener, M. Saeidpour, L. Wadsö, Hydration states of AFm cement phases, Cem. Concr. Res. 73 (2015) 143–157. https://doi.org/10.1016/j.cemconres.2015.02.011.

[123] F. Avet, X. Li, K. Scrivener, Determination of the amount of reacted metakaolin in calcined clay blends, Cem. Concr. Res. 106 (2018) 40–48. https://doi.org/10.1016/j.cemconres.2018.01.009.

[124] S. Adu-Amankwah, M. Zajac, C. Stabler, B. Lothenbach, L. Black, Influence of limestone on the hydration of ternary slag cements, Cem. Concr. Res. 100 (2017) 96–109. https://doi.org/10.1016/j.cemconres.2017.05.013.

[125] R.W. Cheary, A. Coelho, Fundamental parameters approach to x-ray line-profile fitting, J. Appl. Crystallogr. 25 (1992) 109–121. https://doi.org/10.1107/S0021889891010804.

[126] C. Naber, S. Stegmeyer, D. Jansen, F. Goetz-Neunhoeffer, J. Neubauer, The PONKCS method applied for time resolved XRD quantification of supplementary cementitious material reactivity in

hydrating mixtures with ordinary Portland cement, Constr. Build. Mater. 214 (2019) 449–457. https://doi.org/10.1016/j.conbuildmat.2019.04.157.

[127] P.R. de Matos, J.S. Andrade Neto, R.D. Sakata, A.P. Kirchheim, E.D. Rodríguez, C.E.M. Campos, Strategies for XRD quantitative phase analysis of ordinary and blended Portland cements, Cem. Concr. Compos. 131 (2022) 104571. https://doi.org/10.1016/j.cemconcomp.2022.104571.

[128] J. Skocek, M. Zajac, M. Ben Haha, Carbon Capture and Utilization by mineralization of cement pastes derived from recycled concrete, Sci. Rep. 10 (2020) 1–12. https://doi.org/10.1038/s41598-020-62503-z.

[129] P. Padilla-Encinas, A. Palomo, M.T. Blanco-Varela, L. Fernández-Carrasco, A. Fernández-Jiménez, Monitoring early hydration of calcium sulfoaluminate clinker, Constr. Build. Mater. 295 (2021) 123578. https://doi.org/10.1016/j.conbuildmat.2021.123578.

[130] L. Steger, S. Blotevogel, L. Frouin, C. Patapy, M. Cyr, Experimental evidence for the acceleration of slag hydration in blended cements by the addition of $CaCl_2$, Cem. Concr. Res. 149 (2021) 106558. https://doi.org/10.1016/j.cemconres.2021.106558.

[131] C.R. Hubbard, R.L. Snyder, RIR — Measurement and Use in Quantitative XRD, Powder Diffr. 3 (1988) 74–77. https://doi.org/10.1017/S0885715600013257.

[132] R.L. Snyder, The Use of Reference Intensity Ratios in X-Ray Quantitative Analysis, Powder Diffr. 7 (1992) 186–193. https://doi.org/10.1017/S0885715600018686.

[133] C. Unluer, A. Al-Tabbaa, Impact of hydrated magnesium carbonate additives on the carbonation of reactive MgO cements, Cem. Concr. Res. 54 (2013) 87–97. https://doi.org/10.1016/j.cemconres.2013.08.009.

[134] E. Berodier, K. Scrivener, Understanding the filler effect on the nucleation and growth of C-S-H, J. Am. Ceram. Soc. 97 (2014) 3764–3773. https://doi.org/10.1111/jace.13177.

[135] B.H. O'Connor, M.D. Raven, Application of the Rietveld Refinement Procedure in Assaying Powdered Mixtures, Powder Diffr. 3 (1988) 2–6. https://doi.org/10.1017/S0885715600013026.

[136] D. Jansen, C. Stabler, F. Goetz-Neunhoeffer, S. Dittrich, J. Neubauer, Does Ordinary Portland Cement contain amorphous phase? A quantitative study using an external standard method, Powder Diffr. 26 (2011) 31–38. https://doi.org/10.1154/1.3549186.

[137] A.A. Coelho, TOPAS and TOPAS-Academic: An optimization program integrating computer algebra and crystallographic objects written in C++: An, J. Appl. Crystallogr. 51 (2018) 210–218. https://doi.org/10.1107/S1600576718000183.

[138] D. Jansen, A. Spies, J. Neubauer, D. Ectors, F. Goetz-Neunhoeffer, Studies on the early hydration of two modifications of ye'elimite with gypsum, Cem. Concr. Res. 91 (2017) 106–116. https://doi.org/10.1016/j.cemconres.2016.11.009.

[139] E.A. Merritt, To B or not to B: A question of resolution?, Acta Crystallogr. Sect. D Biol. Crystallogr. 68 (2012) 468–477. https://doi.org/10.1107/S0907444911028320.

[140] O. Pritula, L. Smrcˇok, B. Baumgartner, On reproducibility of Rietveld analysis of reference Portland cement clinkers, Powder Diffr. 18 (2003) 16–22. https://doi.org/10.1154/1.1545116.

[141] B.H. Toby, R factors in Rietveld analysis: How good is good enough? , Powder Diffr. 21 (2006) 67–70. https://doi.org/10.1154/1.2179804.

[142] F. Winnefeld, A. Schöler, B. Lothenbach, Sample preparation, in: A Pract. Guid. to Microstruct. Anal. Cem. Mater., 2016: pp. 1–35. https://doi.org/10.7693/wl20150205.

[143] J. Zhang, G.W. Scherer, Comparison of methods for arresting hydration of cement, Cem. Concr. Res. 41 (2011) 1024–1036. https://doi.org/10.1016/j.cemconres.2011.06.003.

[144] R. Snellings, J. Chwast, Ö. Cizer, N. De Belie, Y. Dhandapani, P. Durdzinski, J. Elsen, J. Haufe, D. Hooton, C. Patapy, M. Santhanam, K. Scrivener, D. Snoeck, L. Steger, S. Tongbo, A. Vollpracht, F. Winnefeld, B. Lothenbach, RILEM TC-238 SCM recommendation on hydration stoppage by solvent exchange for the study of hydrate assemblages, Mater. Struct. Constr. 51 (2018). https://doi.org/10.1617/s11527-018-1298-5.

[145] P.R. de Matos, J.S. Andrade Neto, C.E.M. Campos, Is the R index accurate to assess the preferred orientation of portlandite in cement pastes?, Constr. Build. Mater. 292 (2021) 123471. https://doi.org/10.1016/j.conbuildmat.2021.123471.

[146] A. Hakamy, F.U.A. Shaikh, I.M. Low, Characteristics of hemp fabric reinforced nanoclay-cement nanocomposites, Cem. Concr. Compos. 50 (2014) 27–35. https://doi.org/10.1016/j.cemconcomp.2014.03.002.

[147] P. Stutzman, Powder diffraction analysis of hydraulic cements: ASTM Rietveld round-robin results on precision, Powder Diffr. 20 (2005) 97–100. https://doi.org/10.1154/1.1913712.

[148] G. U.S. Department of Commerce, Certificate of Analysis. Standard Reference Material 2686a, Technical Note, National Institute of Standards and Technology, (2012) 1. https://doi.org/https://www-s.nist.gov/srmors/view_detail. cfm?srm=2686A.

[149] M. García-Maté, I. Santacruz, A. Cuesta, L. León-Reina, M.A.G. Aranda, I. Baco, V. Morin, G. Walenta, E. Gartner, Á.G. De La Torre, Amorphous determination in calcium sulfoaluminate materials by external and internal methods, Adv. Cem. Res. 27 (2015) 417–423. https://doi.org/10.1680/adcr.14.00026.

[150] P. Stutzman, Quantitative X-Ray Powder Diffraction Analysis of Portland Cements: Proficiency Testing for Laboratory Assessment, Adv. Civ. Eng. Mater. 3 (2014) 20130093. https://doi.org/10.1520/acem20130093.

[151] L. León-Reina, A.G. De La Torre, J.M. Porras-Vázquez, M. Cruz, L.M. Ordonez, X. Alcobé, F. Gispert-Guirado, A. Larrãaga-Varga, M. Paul, T. Fuellmann, R. Schmidt, M.A.G. Aranda, Round robin on Rietveld quantitative phase analysis of Portland cements, J. Appl. Crystallogr. 42 (2009) 906–916. https://doi.org/10.1107/S0021889809028374.

[152] R. Snellings, J. Chwast, Ö. Cizer, N. De Belie, Y. Dhandapani, P. Durdzinski, J. Elsen, J. Haufe, D. Hooton, C. Patapy, M. Santhanam, K. Scrivener, D. Snoeck, L. Steger, S. Tongbo, A. Vollpracht, F. Winnefeld, B. Lothenbach, Report of TC 238-SCM: hydration stoppage methods for phase assemblage studies of blended cements—results of a round robin test, Mater. Struct. Constr. 51 (2018). https://doi.org/10.1617/s11527-018-1237-5.

[153] A. Cuesta, Á.G. De La Torre, I. Santacruz, A. Diaz, P. Trtik, M. Holler, B. Lothenbach, M.A.G. Aranda, Quantitative disentanglement of nanocrystalline phases in cement pastes by synchrotron ptychographic X-ray tomography, IUCrJ. 6 (2019) 473–491. https://doi.org/10.1107/S2052252519003774.

[154] S. Shirani, A. Cuesta, A. Morales-Cantero, A.G. De la Torre, M.P. Olbinado, M.A.G. Aranda, Influence of curing temperature on belite cement hydration: A comparative study with Portland cement, Cem. Concr. Res. 147 (2021) 106499. https://doi.org/10.1016/j.cemconres.2021.106499.

[155] F. Hueller, J. Neubauer, S. Kaessner, F. Goetz-Neunhoeffer, Hydration of calcium aluminates at 60°C – Development paths of C_2AH_x in dependence on the content of free water, J. Am. Ceram. Soc. 102 (2019) 4376–4387. https://doi.org/10.1111/jace.16314.

[156] H. Hashizume, S. Shimomura, H. Yamada, T. Fujita, H. Nakazawa, O. Akutsu, An X-ray diffraction system with controlled relative humidity and temperature, Powder Diffr. 11 (1996) 288–289. https://doi.org/10.1017/S088571560000926X.

[157] N.V.Y. Scarlett, I.C. Madsen, L.M.D. Cranswick, T. Lwin, E. Groleau, G. Stephenson, M. Aylmore, N. Agron-Olshina, Outcomes of the International Union of Crystallography Commission on Powder Diffraction round robin on quantitative phase analysis: Samples 2, 3, 4, synthetic bauxite, natural granodiorite and pharmaceuticals, J. Appl. Crystallogr. 35 (2002) 383–400. https://doi.org/10.1107/S0021889802008798.

[158] W.A. Dollase, Correction of Intensities of Preferred Orientation in Powder Diffractometry: Application of the March Model., J. Appl. Crystallogr. 19 (1986) 267–272. https://doi.org/10.1107/S0021889886089458.

[159] R.B. Von Dreele, Quantitative texture analysis by Rietveld refinement, J. Appl. Crystallogr. 30 (1997) 517–525. https://doi.org/10.1107/S0021889897005918.

[160] Á.G. De la Torre, M.-G. López-Olmo, C. Álvarez-Rua, S. García-Granda, M.A.G. Aranda, Structure and microstructure of gypsum and its relevance to Rietveld quantitative phase analyses, Powder Diffr. 19 (2004) 240–246. https://doi.org/10.1154/1.1725254.

[161] D. Ectors, Advances in the analysis of cementitious reactions and hydrate phases, Friedrich-Alexander-Universität, 2016. urn:nbn:de:bvb:29-opus4-71743.

[162] Y. Shimada, J.F. Young, Thermal stability of ettringite in alkaline solutions at 80°C, Cem. Concr. Res. 34 (2004) 2261–2268. https://doi.org/10.1016/j.cemconres.2004.04.008.

[163] G. Li, P. Le Bescop, M. Moranville-Regourd, Synthesis of the U phase ($4CaO \cdot 0.9Al_2O_3 \cdot 1.1SO_3 \cdot 0.5Na_2O \cdot 16H2O$), Cem. Concr. Res. 27 (1997) 7–13. https://doi.org/10.1016/S0008-8846(96)00194-9.

[164] S.R. Klaus, J. Neubauer, F. Goetz-Neunhoeffer, Hydration kinetics of CA_2 and CA - Investigations performed on a synthetic calcium aluminate cement, Cem. Concr. Res. 43 (2013) 62–69. https://doi.org/10.1016/j.cemconres.2012.09.005.

[165] R.J. Myers, G. Geng, E.D. Rodriguez, P. da Rosa, A.P. Kirchheim, P.J.M. Monteiro, Solution chemistry of cubic and orthorhombic tricalcium aluminate hydration, Cem. Concr. Res. 100 (2017) 176–185. https://doi.org/10.1016/j.cemconres.2017.06.008.

[166] K. Scrivener, R. Snellings, B. Lothenbach, A Practical Guide to Microstructural Analysis of Cementitious Materials, 2018. https://doi.org/10.1201/b19074.

[167] J. Skibsted, High-resolution solid-state nuclear magnetic resonance spectroscopy of Portland cement-based systems, in: A Pract. Guid. to Microstruct. Anal. Cem. Mater., 2016: p. 2016.

[168] J.M. Arnaud, C. A. Muller, P.J. McDonald, Proton nuclear magnetic resonance relaxometry, in: A Pract. Guid. to Microstruct. Anal. Cem. Mater., CRC press, 2016.

[169] D. Ectors, F. Goetz-Neunhoeffer, W.-D. Hergeth, U. Dietrich, J. Neubauer, In situ 1 H-TD-NMR: Quantification and microstructure development during the early hydration of alite and OPC, Cem. Concr. Res. 79 (2016) 366–372. https://doi.org/10.1016/j.cemconres.2015.10.011.

[170] F. Winnefeld, B. Lothenbach, On the Occurrence of CAH10 in Hydrated Calcium Sulfoaluminate Cements, in: 11th ACI/RILEM Int. Conf. Cem. Mater. Altern. Bind. Sustain. Concr., 2021: pp. 125–142.

[171] F. Bullerjahn, Characterisation and hydration of ye'elimite containing cements, École Polytechnique Fédérale de Lausanne, 2018.

[172] B. Lothenbach, M. Zajac, Application of thermodynamic modelling to hydrated cements, Cem. Concr. Res. 123 (2019) 105779. https://doi.org/10.1016/j.cemconres.2019.105779.

[173] M. Zajac, J. Skocek, F. Bullerjahn, B. Lothenbach, K. Scrivener, M. Ben Haha, Early hydration of ye'elimite: Insights from thermodynamic modelling, Cem. Concr. Res. 120 (2019) 152–163. https://doi.org/10.1016/j.cemconres.2019.03.024.

[174] F. Winnefeld, B. Lothenbach, Hydration of calcium sulfoaluminate cements - Experimental findings and thermodynamic modelling, Cem. Concr. Res. 40 (2010) 1239–1247. https://doi.org/10.1016/j.cemconres.2009.08.014.

[175] T. Manninger, D. Jansen, J. Neubauer, F. Goetz-Neunhoeffer, Phase solubility changes during hydration of monocalciumaluminate and calcite-the influence of alkali accumulation, Materials (Basel). 13 (2020) 1–16. https://doi.org/10.3390/ma13061406.

[176] I.M. Krieger, T.J. Dougherty, A Mechanism for Non-Newtonian Flow in Suspensions of Rigid Spheres, Trans. Soc. Rheol. 3 (1959) 137–152. https://doi.org/10.1122/1.548848.